Quantifying black carbon light absorption enhancement by a novel statistical approach

Cheng Wu[1,2], Dui Wu[1,2,3], Jian Zhen Yu[4,5,6]

[1]Institute of Mass Spectrometer and Atmospheric Environment, Jinan University, Guangzhou 510632, China

[2]Guangdong Provincial Engineering Research Center for on-line source apportionment system of air pollution, Guangzhou 510632, China

[3]Institute of Tropical and Marine Meteorology, China Meteorological Administration, Guangzhou 510080, China

[4]Division of Environment, Hong Kong University of Science and Technology, Clear Water Bay, Hong Kong, China

[5]Atmospheric Research Centre, Fok Ying Tung Graduate School, Hong Kong University of Science and Technology, Nansha, China

[6]Department of Chemistry, Hong Kong University of Science and Technology, Clear Water Bay, Hong Kong, China

Corresponding to: Cheng Wu (wucheng.vip@foxmail.com) and Jian Zhen Yu (jian.yu@ust.hk)

Abstract

Black carbon (BC) particles in the atmosphere can absorb more light when coated by non-absorbing or weakly absorbing materials during atmospheric aging, due to the lensing effect. In this study, the light absorption enhancement factor, E_{abs}, was quantified using one year's measurement of mass absorption efficiency (MAE) in the Pearl River Delta region (PRD). A new approach for calculating primary MAE (MAE_p), the key for E_{abs} estimation, is demonstrated using the Minimum R Squared (MRS) method, exploring the inherent source independency between BC and its coating materials. A unique feature of E_{abs} estimation by the MRS approach is its insensitivity to systematic biases in EC and σ_{abs} measurements. The annual average E_{abs550} is found to be 1.50±0.48 (±1 S.D.) in the PRD region, exhibiting a clear seasonal pattern with higher values in summer and lower in the winter. Elevated E_{abs} in the rainy summer season is likely associated with aged air masses dominating from marine origin, along with long-range transport of biomass burning influenced air masses from Southeast Asia. Core-shell Mie simulations along with measured E_{abs} and Angstrom absorption exponent (AAE) constraints suggest that in the PRD, the coating materials are unlikely to be dominated by brown carbon and the coating thickness is higher in the rainy season than the dry season.

1 Introduction

Originating from incomplete combustion, black carbon (BC) is a crucial constituent of atmospheric aerosols, and is an air pollutant itself, having an adverse health impacts on humans (Suglia et al., 2008). BC has also been recognized as the third most important climate forcer due to its broad light absorbing capability across the UV-Vis-IR spectrum (IPCC, 2013). BC can alter the climate in a variety of ways, including by direct forcing (Bond et al., 2011), affecting cloud cover (Koch and Del Genio, 2010) and precipitation (Tao et al., 2012), reducing the albedo of snow and ice (Hansen and Nazarenko, 2004) and causing surface dimming (Wild, 2011). The climate effects of BC can be global or regional (Ramanathan and Carmichael, 2008). A recent study found BC can modify planetary boundary layer meteorology, and thus enhance local pollution indirectly (Ding et al., 2016). However, due to its variable optical characteristics induced during atmospheric aging, large uncertainties still exist in estimating the radiative forcing from BC. Optical properties of BC can be predicted by knowing the mass concentration, mixing state and size distribution, which collectively serve as the cornerstone for modeling the climate effect of BC. In 3D modeling studies, to conserve computational resources, the mass absorption efficiency (MAE) or mass absorption cross-section (MAC) is widely used to convert black carbon mass concentration to light absorption coefficient (σ_{abs}). MAE is a quantity to describe the light absorption ability per unit EC mass:

$$\text{MAE}\ (m^2\ g^{-1}) = \frac{absorption\ coefficient\ \sigma_{abs}\ (Mm^{-1})}{EC\ mass\ concentration\ (\mu g\ m^{-3})} \quad (1)$$

As a fundamental input parameter, MAE has a critical impact on BC's radiative forcing estimation in climate modeling studies. Mixing state is one of the governing factors affecting MAE. Light absorption of soot particles is enhanced when coated with non-absorbing materials (Fuller et al., 1999) or weakly absorbing materials (Lack and Cappa, 2010) during atmospheric aging. The coating materials can focus more light onto the soot core through the lensing effect, resulting in elevated MAE (Wang et al., 2017). Strong correlations between MAE and the number/volume fraction of coated particles have been reported in urban areas like Tokyo (Naoe et al., 2009), Shenzhen (Lan et al., 2013) and Xi'an (Wang et al., 2014), implying that the elevated MAE observed at these locations was mainly due to the elevated fraction of coated of soot particles. Total absorption ($\sigma_{abs,t}$) of coated particles can

be separated into two parts: primary absorption ($\sigma_{abs,p}$) due to the uncoated soot core alone, and extra absorption ($\sigma_{abs,c}$) due to lensing effect of the coating (Bond et al., 2006; Jacobson, 2006; Liu et al., 2016a) and the presence of secondarily formed brown carbon (BrC) (Lack and Cappa, 2010; Liu et al., 2016b).

$$\sigma_{abs,t} = \sigma_{abs,p} + \sigma_{abs,c} \quad (2)$$

The absorption enhancement factor (E_{abs}) then can be defined as ratio of the total absorption and primary absorption coefficients or the corresponding MAE values:

$$E_{abs} = \frac{\sigma_{abs,t}}{\sigma_{abs,p}} = \frac{MAE_t}{MAE_p} \quad (3)$$

Where MAE_p represents the ratio of $\sigma_{abs,p}/EC$ for uncoated soot particles, similar to the concept of the primary OC/EC ratio in the EC tracer method:

$$MAE_p = \frac{\sigma_{abs,p}}{EC} \quad (4)$$

And the MAE of coated BC can be defined as:

$$MAE_t = \frac{\sigma_{abs,t}}{EC} \quad (5)$$

Thus, elevated MAE induced by coating during atmospheric aging results in an E_{abs} larger than 1.

Previous model studies suggest that absorption by aged soot particles can be 1.5 times greater than fresh soot (Fuller et al., 1999; Bond et al., 2006). Laboratory studies have demonstrated that soot particles coated with SOA (Saathoff et al., 2003; Schnaiter et al., 2005; Tasoglou et al., 2017) and sulfuric acid (Zhang et al., 2008; Khalizov et al., 2009) can increase E_{abs}. An artificial coating experiment by Shiraiwa et al. (2010) found an E_{abs} of 2 for graphite particles growing in diameter from 185 to 370 nm. A laboratory study by McMeeking et al. (2014) found that in the presence of BrC, light absorption enhancement is more pronounced at the shorter wavelength. A recent chamber study coupling actual ambient air with seed BC particles implies that the timescale for E_{abs} reaching 2.4 is only 5 hours in Beijing but 18 hours in Houston (Peng et al., 2016). Field studies conducted in recent years have also substantiated enhanced light absorption in Canada (Knox et al., 2009; Chan et al., 2011), US (Lack et al., 2012b), UK (Liu et al., 2015) and Japan (Nakayama et al., 2014; Ueda et al.,

2016). In contrast, field studies in California, US (Cappa et al., 2012) found a weaker light absorption enhancement (6% on average). A recent study suggests the mass ratio of non-BC content to BC particles determines the occurrence of the absorption enhancement of black-carbon particles (Liu et al., 2017).

Two approaches are widely used to determine E_{abs} from ambient measurements. The first approach removes the coating materials on particles physically using a thermal denuder (TD) (Lack et al., 2012a) or by aerosol filter filtration-dissolution (AFD) (Cui et al., 2016b). The TD approach is briefly discussed here. Coating materials can be removed by TD at a working temperature around 200 to 300 °C (depending on the charring characteristics of aerosols at the sampling site) to measure $\sigma_{abs,p}$, which are cycled with measurements of $\sigma_{abs,t}$ (without passing through TD), allowing E_{abs} to be obtained from the ratio of $\sigma_{abs,t}/\sigma_{abs,p}$ following Eq.3. The major advantage of the TD approach is its ability to provide highly time resolved measurements (minutes). A photo-acoustic spectrometer (PAS) is commonly used with TD for detection to satisfy its high time resolution demands. As an in-situ technique, PAS eliminates the artifacts associated with filter-based methods (Weingartner et al., 2003; Coen et al., 2010) and is often considered as the reference instrument for light absorption coefficient determination (Arnott et al., 2003; Arnott et al., 2005). One limitation of the TD approach is that a universal optimal operation temperature does not exist, leading to a chemical composition dependent efficiency. If the temperature is too low, the coating cannot be fully removed, and charring can occur if the TD temperature is too high, leading to biased results. For example, a SP-AMS study in Toronto found that the efficiency of BC coating removal by TD decreased substantially for wildfire influenced samples (Healy et al., 2015). Another issue is particle loss due to TD, which can be ~ 20% and needs to be taken into account (Ueda et al., 2016). It's also worth noting that MAE_p by the TD approach is different from the MAE_p at the emission source. First, the morphology of thermally denuded BC particles (compact aggregates) is different from that of freshly emitted BC particles (chain-like aggregates). Second, most of the coatings is removed with the TD denuded soot particles, but freshly emitted soot particles usually come with a thin coating of OC formed from condensation of OC vapors as the temperature drops from engine to the ambient air. As a result, the MAE_p by TD

approach is expected to be lower than the MAE_p of emission source. In this sense, the TD approach may not be a prefect "time machine" to reverse the aging process for E_{abs} determination.

The second approach is the MAE ratio method, which is also stated in Eq. 3. The key to this method is determining an appropriate MAE_p that can represent the MAE from primary emissions. One approach is to adopt the reference MAE_p from the literature but it may fail to represent the actual MAE_p at a specific sampling site, since MAE_p varies temporally and spatially. For example, MAE_p of diesel soot was found to be 7.1 m^2g^{-1} at 532 nm (Adler et al., 2010). A much higher MAE_p (16 m^2g^{-1} at 530 nm) was observed from natural gas flaring (Weyant et al., 2016). MAE_p of biomass burning (BB) samples is highly varied due to a wide range of fuel types and combustion conditions (Reid et al., 2005; Roden et al., 2006). A range from 6.1 to 80.8 m^2g^{-1} was reported for BB MAE_p at 550 nm (Pandey et al., 2016). Without the knowledge of source contributions, it is not feasible to derive a representative MAE_p for E_{abs} estimation. The other commonly used approach is to determine MAE_p from the dependency of MAE on the number fraction of coated soot particles measured by SP2 (Lan et al., 2013). Since MAE (y axis) is positively correlated with the number fraction of coated soot particles (x axis), MAE_p can be determined by extending the regression line to x=0. It is worth noting that this approach provides only a rough approximation of E_{abs} since the parameter used here (coated soot particles number fraction) ignores other main drivers of light absorption enhancement (e.g. coating thickness). As a result, this approach is only valid for a period of measurements, for which coating thickness is relatively constant and the MAE variations are dominated by coated soot particles number fraction.

However, the high cost of the TD-PAS system and SP2 limit the field measurement of E_{abs} around the world. In addition, long-term E_{abs} measurements by a TD-PAS system and SP2 are not easily achieved and rarely reported. On the other hand, an Aethalometer and RT-ECOC analyzer can be effectively deployed for long term measurements and E_{abs} estimation, at a relatively lower cost. In this study, based on one year of hourly MAE measurements (with the field carbon analyzer and Aethalometer) at a suburban site in the Pearl River Delta (PRD) region of China, quantification of MAE_p is demonstrated by a novel statistical approach, the Minimum R squared method (MRS) (Wu and Yu, 2016). The aim of this study is to demonstrate the capability of E_{abs} estimation using a year-

long dataset from cost-effective instrumentation. The seasonal variability of MAE, AAE and E_{abs} in the PRD region are characterized and their dependency on air mass origin and biomass burning are discussed. Abbreviations used in this study are summarized in Table 1 for a quick lookup.

2 Ambient measurements

Sampling was conducted from Feb 2012 to Jan 2013 at the suburban Nancun (NC) site (23° 0'11.82"N, 113°21'18.04"E). NC, situated on the top of the highest peak (141 m ASL) in Guangzhou's Panyu district, is located at the geographic center of the PRD region, making it a representative location for average atmospheric mixing characteristics of city clusters in the PRD region. Light absorption measurements were performed by a 7-λ Aethalometer (AE-31, Magee Scientific Company, Berkeley, CA, USA). The Aethalometer was equipped with a 2.5 μm cyclone with a sampling flow rate of 4 L min^{-1}. Weingartner's algorithm (Weingartner et al., 2003) was adopted to correct the sampling artifacts (aerosol loading, filter matrix and scattering effect) rooted in filter based method. A customized Aethalometer data processing program (Wu, 2017a) with graphical user interface was developed to perform data correction and detailed descriptions can be found in the SI (The program is available from https://sites.google.com/site/wuchengust). Details of the Aethalometer setup and data correction can be found in our previous paper (Wu et al., 2013).

EC mass concentrations were determined by a real time ECOC analyzer (Model RT-4, Sunset Laboratory Inc., Tigard, Oregon, USA). The sunset carbon analyzer was sampling on hourly cycles at a flow rate of 8 $Lmin^{-1}$ with a $PM_{2.5}$ sharp-cut cyclone inlet. For each measurement hour, the first 45min were for sample collection and the remaining 15 min for thermal-optical analysis. OC is volatized first by step-wise temperature ramping in an oxygen-free atmosphere while in the second stage EC is combusted in the presence of oxygen. Laser transmittance is applied to correct the charring artifact during the OC stage.

Considering a measurement precision of 5% for the Aethalometer (Hansen, 2005) and 24% for the RT-ECOC analyzer (Bauer et al., 2009), the propagated relative precision of E_{abs} ($E_{abs,Unc}$) is 35% following Eq. S1&S2 in the SI. It should be noted that $E_{abs,Unc}$ is mainly attributed to the

measurement precision of EC by the RT-ECOC analyzer. Since the measurement precision of the RT-ECOC analyzer estimated by Bauer et al. (2009) is obtained from field measurement at an environment (EC below 1 μg m^{-3}) where EC is much lower than the present study (annual average EC 2.66±2.27 μg m^{-3}), the $E_{abs,Unc}$ of 35% should be considered as an upper limit for the present study.

Light scattering was measured by an integrating nephlometer (Aurora-1000, Ecotech, Melbourne, Australia). Water soluble ions were measured by MARGA (The instrument for Measuring AeRosols and GAses)(ten Brink et al., 2007). Both instruments are equipped with a $PM_{2.5}$ inlet to remove the coarse particles.

2.1 Uncertainties of MAE determination

Two major uncertainties associated with the σ_{abs} and EC determination techniques should be taken into account when comparing MAE across different studies. For the σ_{abs} determination technique, photo-acoustic spectroscopy (PAS) is an in-situ technique free from filter based artifacts, but its application is limited by its high cost. The filter based optical transmittance method (e.g., Aethalometer and Multi Angle Absorption Photometer, MAAP) is the most widely used technique around the world, but data correction is needed to minimize the bias from artifacts due to the loading effect, matrix effect and scattering effect (Weingartner et al., 2003; Arnott et al., 2005; Schmid et al., 2006; Virkkula et al., 2007; Coen et al., 2010; Drinovec et al., 2017; Saturno et al., 2017). Besides these artifacts, RH is also a source of σ_{abs} measurement uncertainty. Elevated RH is not only a driving force of increased σ_{abs} due to the hygroscopic growth of particles, but also a factor affecting ambient σ_{abs} measurements. Previous studies found σ_{abs} by PAS exhibit a systematic decrease when RH>70% (Arnott et al., 2003; Kozlov et al., 2011). Water evaporation was found as the major cause for the biased PAS σ_{abs} measurements under high RH (Raspet et al., 2003; Lewis et al., 2009b; Langridge et al., 2013). Filter-based measurements are also affected under high RH conditions. For example, Arnott et al. (2003) observed erratic responses by particle soot absorption photometer (PSAP) as RH changed. The main reason is traced to the hydrophilic cellulose membrane, which serves to reinforce the quartz filter used in PSAP. The fibers can swell and shrink as RH changes, causing unwanted light attenuation signal. The PTFE-coated glass-fiber tape has become available since 2012 for the recent model of Aethalometer to minimize the RH interference (Magee-Scientific, 2017). A study by Schmid et al. (2006) reported dependency of PSAP σ_{abs} on RH, but found negligible effect of RH on Aethalometer performance. It is also worth noting that RH in the Aethalometer optical chamber may be lower than

196 the ambient RH due to the slightly elevated temperature inside the instrument. The magnitude of RH
197 difference was found similar between different instruments: 20% for the Aethalometer (Schmid et al.,
198 2006) and 15% for the nephelometer (Guyon et al., 2004). The RH in the Aethalometer optical chamber
199 was not measured in this study. We expected its level to be slightly lower than the ambient RH. Cappa
200 et al. (2008) found σ_{abs} measurements by PSAP and PAS maintained a high linearity even under high
201 RH conditions (65-91%). Inter-comparison studies demonstrated that with proper corrections,
202 Aethalometer σ_{abs} measurements agree well with those by PAS (Ajtai et al., 2011). During the inter-
203 comparison study of an Aethalometer (AE-16) and a PAS in Guangzhou (Wu et al., 2009), good
204 correlation was found (R^2=0.96) as shown in Figure S1. These comparison results imply that the
205 Aethalometer results are linearly correlated with PAS measurements and RH has a limited interference
206 on Aethalometer measurements. In our study, careful corrective measures (Wu et al., 2013) are
207 conducted for the Aethalometer σ_{abs} data treatment to minimize these artifacts. But such artifacts
208 still cannot be fully eliminated.

209 For the EC determination, different thermal optical analysis (TOA) protocols can impact the
210 measurement variability and thus MAE. As shown in Table S1, MAE for the same samples at Fresno
211 varied from 6.1 to 9.3 $m^2 g^{-1}$, depending on which EC analysis protocol was applied (Chow et al.,
212 2009). Studies in the PRD found that discrepancies in measured EC by different analysis protocols
213 could be as large as a factor of 5 (Wu et al., 2012; Wu et al., 2016a), which adds to the uncertainty for
214 the MAE estimation. In addition, EC by TOA is also different from refractory BC (rBC) reported by
215 the laser induced incandescence (LII) technique (e.g. single particle soot photometer, SP2). For
216 example, two studies in Toronto (Knox et al., 2009; Chan et al., 2011) both used the PAS for σ_{abs}
217 measurement but different techniques for EC mass determination, resulting in very different MAE
218 results. LII instruments are usually calibrated with a commercially available surrogate (e.g. fullerene)
219 since direct calibration with ambient soot is not easy to achieve. Laborde et al. (2012) indicates that
220 the incandescence response of SP2 exhibits a dependency on soot type (15% between fullerene and
221 denuded diesel soot particles; 14% between biomass burning and denuded diesel soot particles). Due
222 to the absence of widely accepted reference materials for EC, the uncertainties in EC determination
223 will exist in the foreseeable future. All these uncertainties, including the uncertainty of rBC mass
224 determination by SP2, uncertainty of EC in TOA, the discrepancy between SP2 rBC and TOA EC and

the discrepancy of σ_{abs} between filter transmission and photo-acoustic methods, can contribute to the differences in MAE listed in Table S1.

Systematic bias in MAE (e.g. overestimation of σ_{abs} and variability of EC mass by different TOA protocols) discussed above have little effect on E_{abs} estimation by MRS. As shown in Eq. 3, E_{abs} is the ratio of MAE_t to MAE_p or $\sigma_{abs,t}$ to $\sigma_{abs,p}$, thus most of the bias in EC mass or σ_{abs} is cancelled out during the E_{abs} calculation. More details are discussed in section 4.1.

3 Methodology

3.1 MAE_p estimation by MRS from the ambient data

In this section, a new approach for MAE_p estimation is introduced for E_{abs} determination, which requires the knowledge of differentiating $\sigma_{abs,p}$ and $\sigma_{abs,c}$ portions in $\sigma_{abs,t}$. The idea of decoupling $\sigma_{abs,t}$ into $\sigma_{abs,p}$ and $\sigma_{abs,c}$ is conceptually similar to decoupling OC into primary OC (POC) and secondary OC (SOC) in the EC tracer method as shown in Table 2. In the EC tracer method, if $(OC/EC)_p$ is known, POC can be determined from OC (Turpin and Huntzicker, 1991). The role of MAE_p here is similar to the role of $(OC/EC)_p$, the primary OC/EC ratio in the EC tracer method (a comparison is given in Table 2). If MAE_p (average MAE from primary emission sources) is known, E_{abs} can be obtained from the ratio of MAE_t/MAE_p (Eq. 3). Therefore, the key for E_{abs} estimation is to derive an appropriate MAE_p. It is worth noting that MAE_p here does not represent MAE from a single or specific primary emission source, instead it reflects an average and effective MAE that has taken consideration of various primary emission sources. Thus, the MAE_p is conceptually analogous to $(OC/EC)_p$ in the EC tracer method, in which the primary ratio reflects an overall ratio from primary emission sources rather than from a single primary source.

The Minimum R squared method (MRS) explores the inherent independency between pollutants from primary emissions (e.g., EC) and products associated with secondary formation processes (e.g., SOC, $\sigma_{abs,c}$) to derive the primary ratios (e.g., $(OC/EC)_p$, MAE_p) in the EC tracer method (Wu and Yu, 2016). When applying MRS for light absorption enhancement estimation, MRS is used to explore the inherent independency between EC and $\sigma_{abs,c}$, which is gained during

atmospheric aging after emission. An example of MAE_p estimation by MRS is shown in Figure 1. Firstly, the assumed MAE_p value is varied continuously in a reasonable range (0.01 to 50 $m^2\ g^{-1}$ as shown in Figure 1). Then at each hypothetical MAE_p, $\sigma_{abs,c}$ can be calculated by Eq. 6 (a combination of Eq. 2&4) using EC and $\sigma_{abs,t}$ from ambient measurements.

$$\sigma_{abs,c} = \sigma_{abs,t} - MAE_p \times EC \quad (6)$$

Accordingly, for each hypothetical MAE_p, a correlation coefficient value (R^2) of $\sigma_{abs,c}$ vs. EC (i.e., $R^2(\sigma_{abs,c}, EC)$) can be obtained. The series of $R^2(\sigma_{abs,c}, EC)$ values (y axis) are then plotted against the assumed MAE_p values (x axis) as shown by the red curve in Figure 1. The physical meaning of this plot can be interpreted as follows. The $\sigma_{abs,p}$ is the fraction of light absorption owing to primary emitted soot particles. As a result, $\sigma_{abs,p}$ is well correlated with EC mass. In contrast, the $\sigma_{abs,c}$ is the fraction of light absorption gained by the lensing effect of the coating on particles after emission. The variability of $\sigma_{abs,c}$ mainly depends on the coating thickness of the soot particles. Consequently, $\sigma_{abs,c}$ is independent of EC mass. Since variations of EC and $\sigma_{abs,c}$ are independent, the assumed MAE_p corresponding to the minimum $R^2(EC, \sigma_{abs,c})$ would then represent the most statistically probable MAE_p of the tested dataset.

A computer program (Wu, 2017b) in Igor Pro (WaveMetrics, Inc. Lake Oswego, OR, USA) was developed to facilitate MRS calculation with a user friendly graphical user interface. Another two Igor Pro based computer programs Histbox (Wu, 2017c) and Scatter Plot (Wu, 2017d) are used for generating histograms, box plots and scatter plots (with Deming regressions) presented in this study. Detailed descriptions of these computer programs can be found in the SI and the computer programs are available from https://sites.google.com/site/wuchengust.

3.2 Mie simulation

It can be informative to model a single soot particle using Mie theory (Bohren and Huffman, 1983) and understand the theoretical range and variability of the soot particle's optical properties. Three types of mixing state are widely employed for parameterization: internal mixing, external mixing and core-shell. To better represent the real situation (coating due to the aging process), a core-

277 shell model is considered in the Mie calculation (Figure S2), which is more realistic than a volume
278 mixture model (Bond et al., 2006). An aerosol optical closure study in the North China Plain (NCP)
279 found that the core-shell model can provide better performance than assuming purely internal mixing
280 and external mixing (Ma et al., 2012). A morphology study using Scanning Transmission X-ray
281 Microscopy found that core-shell is the dominating mixing state in ambient samples (Moffet et al.,
282 2016). It should be noted that the core-shell model assumption still has its own limitations. A single
283 particle soot photometer (SP2) study by Sedlacek et al. (2012) reported a negative lag time between
284 the scattering and incandescence signals in samples influenced by biomass burning, implying a near
285 surface location of soot relative to non-absorbing materials. Near surface type mixing of soot has also
286 been observed in Tokyo, but accounted for only 10% of total mixed soot containing particles (Moteki
287 et al., 2014). Considering the domination of core-shell type particles in the ambient environment, the
288 core-shell assumption in our optical model is sufficient to approximate the real situation.

289 As shown in Figure S2, fresh emitted soot particles are chain-like aggregates of small spheres
290 (30~50 nm). After the aging process, soot particles are coated with organic and inorganic materials.
291 Sufficient evidence has shown that the coating not only results in particle size growth, but also makes
292 the soot core become more compact due to its collapse (Alexander et al., 2008; Zhang et al., 2008;
293 Lewis et al., 2009a), especially under high RH conditions (Leung et al., 2017). A recent study by Pei
294 et al. (2017) shown that filling of void space within the agglomerate is the first step of the
295 morphological transformation of soot particles in atmospheric aging, leading to a spherical soot core.
296 Since the spherical like core and shell favor Mie simulation, both core and shell are considered as
297 spheres in the Mie calculation.

298 To investigate the spectrum properties of soot particles, 11 wavelengths (370, 405, 470, 520,
299 532, 550, 590, 660, 781, 880 and 950 nm) are considered in calculations to cover wavelengths in the
300 most frequently used absorption measurement instruments. A refractive index (RI) of 1.85 – 0.71i is
301 adopted for soot core (Bond and Bergstrom, 2006) and 1.55 for non-absorbing coating (clear shell) in
302 the Mie calculation for all wavelengths. Studies suggest a group of organic matter (OM), known as
303 Brown Carbon (BrC), can absorb solar radiation at UV wavelengths (Kirchstetter et al., 2004). Thus,
304 a BrC coating (brown shell) scenario is also considered in Mie simulation following the wavelength-

dependent RI suggested by Lack and Cappa (2010), which ranges from 1.55-0.059i (370 nm) to 1.55-0.0005i (950 nm). A modeling study by Bond et al. (2006) indicates that absorption amplification is not sensitive to the RI, thus the result below is not expected to be sensitive to the RI variability. Due to the spherical assumption of the BC core, a constant particle density is adopted for simplicity instead of size dependent particle density. But it is worth noting that in reality, the effective density of soot varies with particle size due to the morphology change during particle aging (Tavakoli and Olfert, 2014; Dastanpour et al., 2017). Both core diameters (D_{core}) and shell diameters (D_{shell}) are constrained in the range of 10 ~ 3000 nm in the model simulations. The Mie calculations are implemented with a customized program (Wu, 2017e) written in Igro Pro (WaveMetrics, Inc. Lake Oswego, OR, USA) and it is available from https://sites.google.com/site/wuchengust. It should be noted that the core-shell type mixing state of particles is still rare in 3D atmospheric models like WRF-Chem (Matsui et al., 2013; Nordmann et al., 2014) due to computational cost limitation.

3.2.1 Mie modeled absorption angstrom exponent (AAE)

Absorption Angstrom Exponent (AAE) is a widely used parameter that describes the wavelength dependence of aerosol light absorption (Moosmuller et al., 2011), which can be written explicitly as

$$AAE(\lambda_1, \lambda_2) = -\frac{\ln(\sigma_{abs,\lambda 1}) - \ln(\sigma_{abs,\lambda 2})}{\ln(\lambda_1) - \ln(\lambda_2)} \quad (7)$$

It is well known that ambient soot particles exhibit an AAE close to unity (Bond, 2001). Modeled variability in $AAE_{470\text{-}660}$ of bare soot particles is shown in Figure S3. For soot particles with D_{core} <200 nm, $AAE_{470\text{-}660}$ is very close to 1 and decreases significantly for particles with D_{core} >200 nm. Considering a typical D_{core} of fresh emitted soot particles smaller than 200 nm (Rose et al., 2006; China et al., 2013), the model results confirm the frequently observed AAE close to 1 from ambient measurements (Kirchstetter et al., 2004). Modeled variability in $AAE_{470\text{-}660}$ of soot particles coated by non-absorbing substances (clear shell) and weakly absorbing materials (brown shell) is shown in Figure 2. Elevated AAE to ~2 is observed in the clear shell scenario (Figure 2a and 3b) for the most probable soot core particle sizes (<200 nm), which agrees well with a previous model study (Lack and

Cappa, 2010), implying that elevated AAE cannot be exclusively attributed to mixing with BrC. AAE elevation is more pronounced in the brown shell scenario. For soot particles with D_{core} <200 nm, brown shell $AAE_{470\text{-}660}$ can easily reach 3 for a coating of D_{shell}/D_{core}=3 (Figure 2c and 2d). These high AAE results are consistent with the previous model study (Lack and Cappa, 2010) and could partially explain the high AAE observed in measurement studies (Kirchstetter et al., 2004; Hoffer et al., 2006), since the presence of externally mixed BrC particles also contribute to the wavelength dependent light absorption.

3.2.2 Mie modeled single scattering albedo (SSA)

Variability in modeled SSA_{525} of soot particles coated by non-absorbing substances and weakly absorbing materials (e.g. BrC) is shown in Figure S4. For particles with D_{core}<200 nm and D_{shell}/D_{core} <3, the SSA increases gradually (up to ~0.9) with a thicker coating and behaves similarly between clear shell and brown shell scenarios.

3.2.3 Mie modeled mass absorption efficiency (MAE)

MAE is a useful indicator for soot mixing state. Variability in MAE of bare soot particles as a function of particle size at a wavelength of 550 nm is illustrated in Figure S5. The magnitude of MAE is sensitive to the soot density assumption, especially for particles <200 nm (Figure S5), but the overall trend of particle size dependency is similar between different density scenarios. MAE peaks at a particle size of 200 nm and decreases dramatically for larger particles. In our MAE calculation, a soot density of 1.9 g cm^{-3} is adopted, as suggested by Bond and Bergstrom (2006). The purpose of adopting constant density is to simplify the MAE calculation. It should be noted that the effective density of soot core is highly variable in ambient environments. For example, a study in Beijing (Zhang et al., 2016b) found a value of 1.2 g cm^{-3}. A recent chamber study found the effective density of soot can evolve from 0.43 to 1.45 g cm^{-3} during aging as coated by m-Xylene oxidation products (Guo et al., 2016). A study by a single-particle aerosol mass spectrometer in Guangzhou found the effective density of soot increased with particle size in the range of 400 to 1600 nm (Zhang et al., 2016a). The MAE of coated particles from different core/shell diameter combinations are shown in Figure S6. For

thickly coated particles, the MAE in the clear shell scenario varied as D_{shell}/D_{core} increased, but the MAE of brown shell scenario increased quasi-monotonously with D_{shell}/D_{core}.

3.2.4 Mie modeled light absorption enhancement factor (E_{abs})

E_{abs} is a better indicator for soot mixing state than MAE since it does not rely on the soot density assumption and is more suitable for comparing Mie simulations with ambient measurements. Modeled variability in E_{abs} of soot particles coated by non-absorbing substances and weakly absorbing materials (e.g. BrC) is shown in Figure 3a and 3c respectively. E_{abs} is not only sensitive to the core/shell diameter combination, but also behaves very differently on the clear and brown shell assumptions. For the clear shell scenario, when D_{coat}/D_{core} <2, E_{abs} does not exceed 2 for particles with different soot core sizes, but for the same D_{coat}/D_{core}, a larger soot core size yields a higher E_{abs} (Figure 3b, cross-sections of Figure 3a). If D_{coat}/D_{core} >2, E_{abs} could be 3 to 5 for particles with a soot core smaller than 200 nm, but for particles with a soot core larger than 200 nm, the E_{abs} is limited to ~2 as shown in Figure 3b. For the brown shell scenario, E_{abs} increased quasi-monotonically with D_{coat}/D_{core}, and this trend is similar for different soot core sizes (Figure 3d). The main reason behind is that in the brown shell scenario, both lensing effect and BrC absorption contribute to E_{abs}. As shown in Figure S7, the BrC absorption contribution to total E_{abs} strongly depends on coating thickness and is insensitive to soot core diameters. When the coating is relatively thin (<5 nm for λ@370 nm, <15 nm for λ@550 nm and <40 nm for λ@880 nm), BrC absorption contribution to the total E_{abs} is less than 20%. As the coating increases to a certain level (~15 nm for λ@370 nm, ~35 nm for λ@550 nm and ~90 nm for λ@880 nm), BrC absorption contribution is comparable to the lensing effect contribution, each contributing ~50% to the total E_{abs}. When the BrC coating is sufficiently thick (>30 nm for λ@370 nm, >90 nm for λ@550 nm and >110 nm for λ@880 nm), BrC absorption dominates the E_{abs} contribution. As a result, if BrC coating is indeed present in ambient samples, a strong wavelength dependent E_{abs} could be observed, since a BrC coating of 30 nm would be enough to induce a large amount of detectable E_{abs} in the UV range. Another major difference between the clear and brown shell scenarios is that, for thickly coated particles (e.g. D_{coat}/D_{core} >2), the brown shell can yield a much higher E_{abs} than the clear shell.

Both primary soot size distribution and coating thickness can affect the absorption enhancement of ambient BC particles. Ambient measurements by LII found soot particle number and mass modes peaking at 110 nm and 220 nm, respectively, in the PRD (Huang et al., 2011). A study in Shanghai found similar results (70 nm for number concentrations and 200 nm for mass concentrations)(Gong et al., 2016). Considering that the LII technique is specific for BC mass determination which is independent of BC mixing state, the size distribution reported by LII can represent the size distribution of the BC core. A study using a Micro Orifice Uniform Deposit Impactor (MOUDI) found a EC mass size distribution in the PRD exhibiting three modes peaking at ~300, ~900 and ~5000 nm (Yu et al., 2010), implying a substantial coating of BC particles, and a diameter amplification of 3. BC sizing by LII is based on volume equivalent diameter (VED), while MOUDI is based on aerodynamic diameter. As a result, these two techniques do not necessarily yield similar sizes, even for the bare soot particles. The conversion between these two types of diameters involves the knowledge of particle density and morphology (drag force). A recent closure study on BC mixing state in the PRD region suggests σ_{abs} is dominated by coated soot particles in the range of 300~400 nm (Tan et al., 2016). Considering the dominant BC core distribution measured by SP2 (110 nm), the upper limit of E_{abs} in the PRD is roughly estimated as ~2 for the clear shell scenario (Figure 3b).

4 Results and discussions

4.1 Annual measurement statistics

The frequency distribution (log-normal) of σ_{abs550} is shown in Figure 4a, with an annual average (±1 S.D.) of 42.65±30.78 Mm^{-1}. A log-normal distribution is also found in the EC mass concentration (Figure 4b), with an annual average of 2.66±2.27 μg m^{-3}. Figure 4c demonstrates the yearlong frequency distribution of MAE_{550} at the NC site. The annual average MAE_{550} is 18.75±6.16 $m^2 g^{-1}$ and the peak (±1 S.D.) of the lognormal fit is 15.70±0.22 $m^2 g^{-1}$. A good correlation is observed between σ_{abs} and EC mass (R^2=0.92) as shown in Figure 4d, and the color coding indicates a MAE dependency on RH, which agrees with a study in Xi'an(Wu et al., 2016b). Annual average $AAE_{470\text{-}660}$ is 1.09±0.13 (Figure S8a), indicating that soot is the dominant absorbing substance in the PRD and the brown shell

scenario shown in the Mie simulation is unlikely to be important. Annual mean SSA_{525} is 0.86±0.05 (Figure S8c), similar to previous studies in the PRD (Jung et al., 2009; Wu et al., 2009). For comparison purpose, MAE measured at original wavelength and MAE scaled to 550 nm following the λ^{-1} assumption are both shown in Table S1. The MAE comparisons discussed below are MAE at 550 nm. MAE_{550} by previous studies at various locations was found to cover a wide range, from 5.9 to 61.6 $m^2\ g^{-1}$. Annual average observed MAE_{550} at NC (18.75 $m^2\ g^{-1}$) is higher than many studies shown in Figure 5, e.g., Shenzhen (Lan et al., 2013), Beijing (Yang et al., 2009), Mexico city (Doran et al., 2007) and Fresno (Chow et al., 2009).

As shown in Figure 1, the annual average $MAE_{p,550}$ estimated by MRS is 13 $m^2\ g^{-1}$. MAE_p by MRS represents the MAE_p at the emission source, which is different from the MAE_p by the TD approach for two reasons. First, the morphology of thermally denuded BC particles (compact aggregates) is different from that of freshly emitted BC particles (chain-like aggregates). Second, most of the coatings are removed for TD denuded soot particles, but freshly emitted soot particles usually come with a thin coating of OC formed from condensation of OC vapors as the temperature drops from the flame to the ambient air. As a result, the MRS-derived MAE_p is expected to be higher than the MAE_p by the TD approach. The estimated $MAE_{p,550}$ is higher than a previous study in Guangzhou (7.44 $m^2\ g^{-1}$) (Andreae et al., 2008), but comparable to Xi'an (11.34 $m^2\ g^{-1}$) (Wang et al., 2014) and Toronto (9.53~12.57 $m^2\ g^{-1}$) (Knox et al., 2009). The annual average E_{abs550} by MRS following Eq. 3 is estimated to be 1.50±0.48 (mean ± 1 S.D.).

As mentioned in section 1, the definition of MAE_p by the TD approach is different from the MAE_p of emission source. The TD MAE_p is expected to be slightly lower than the MAE_p of emission source. Therefore, the corresponding E_{abs} are slightly different and it should be cautioned when comparing MRS-derived E_{abs} with E_{abs} by the TD approach and Mie simulations. The E_{abs} could vary by location, depending on the coating thickness and size distribution of the primary aerosols. After undergoing atmospheric aging, the E_{abs} can be increased during transport from emission source to rural areas. The magnitude of the E_{abs} found at the NC site is comparable to other locations such as Boulder (Lack et al., 2012a) (1.38), London (Liu et al., 2015) (1.4), Shenzhen (Lan et al., 2013) (1.3), Yuncheng (Cui et al., 2016b) (2.25), Jinan (Chen et al., 2017) (2.07) and Nanjing (Cui et al., 2016a) (1.6) and is

higher than studies in California (Cappa et al., 2012) (1.06), as listed in Table 3. Spectrum E_{abs} are calculated from 370 to 950 nm as shown in Figure S9. E_{abs} in the PRD exhibits a weak wavelength dependence, with slightly higher E_{abs} at the shorter wavelength (e.g. E_{abs370} = 1.55±0.48) and is relatively lower in the IR range (e.g. E_{abs950} = 1.49±0.49).

4.2 Monthly characteristics of MAE, AAE and SSA

Monthly variations of MAE_{550} at the NC site are shown in Figure 6a and Table S2, revealing distinct patterns of higher MAE_{550} in summer and lower in winter. On the other hand, $AAE_{470\text{-}660}$ is lower in summer and higher in winter (Figure 6b and Table S3). Monthly SSA_{525} varied from 0.83 to 0.90 without a clear seasonal pattern, as shown in Figure S10 and Table S4. $MAE_{p,550}$ estimation for individual months is shown in Figure 6a (the purple line) and monthly E_{abs550} is calculated accordingly following Eq. 3 (Figure 6c). E_{abs550} shows clear seasonal variations, with higher values from April to August (1.52~1.97 as shown in Table S5) and relatively lower values from September to March (1.24~1.49). The highest enhancement is found in August (1.97). Factors affecting variation of E_{abs550} are discussed in the following sections, including air mass origin and biomass burning.

4.3 The effect of air mass origin

It's of interest to understand the seasonal variations of optical properties in the PRD. Hourly backward trajectories for the past 72 hours were calculated using NOAA's HYSPLIT (Hybrid Single Particle Lagrangian Integrated Trajectory, version 4) model (Draxier and Hess, 1998) from Feb 2012 to Jan 2013 as shown in Figure S11. Cluster analysis was conducted using MeteoInfo (Wang, 2014). By examining the total spatial variance (TSV), the number of clusters was determined to be four as shown in Figure S12. Cluster 1 (C1) represents continental air masses from the north, accounting for 44.4% of total trajectories. C2 (22.8%) represents marine air masses coming from the South China Sea. C3 represents air masses from the east (Taiwan island). C4 (15.8%) represents transitional air masses coming from the east coastline of China. As shown in Figure 7, E_{abs550} from C2 (1.78) is higher than other clusters (1.30 – 1.42). Further Wilcoxon-Mann-Whitney tests show that E_{abs550} from C2 is significantly higher than E_{abs550} from C1, C3 and C4 (Figure S13), implying that particles from the

South China Sea cluster is likely more aged than other clusters. Air mass origin in the PRD is dominated by C2 from Apr to Aug (Figure S14a) as a result of the South China Sea monsoon in the rainy season. In contrast, the dry season is ruled by continental air masses from the north (C1) due to the influence of the northeast monsoon. E_{abs550} from C2 varied from 1.67 to 2.19, but was always higher than E_{abs550} from C1 and C3 during the rainy season (Figure S14b). As a result, the domination of aged air mass from the vast ocean is one of the reasons for the much higher E_{abs550} found in the rainy season.

4.4 The effect of biomass burning

Biomass burning (BB) and vehicular emission are the two major sources of soot particles. BC from biomass burning emission, depending on the fuel type and burning condition, may have a higher OC/EC ratio and a thicker coating, resulting in a higher MAE than vehicular emission (Shen et al., 2013; Cheng et al., 2016) . In this study, the influence of BB on optical properties is investigated using the K^+/EC ratio as a BB indicator. As shown in Figure 8, MAE_{550} is positively correlated with the K^+/EC ratio, which exhibits a clear seasonal pattern that is higher in the rainy season and lower in the dry season (Figure S15a). Southeast Asia has the highest fire emission density globally due to the high biofuel consumption along with frequent fire activity in this region (Aouizerats et al., 2015), making Southeast Asia a large contributor to BC emissions (Jason Blake, 2014). During the rainy season when oceanic wind prevails, BC from BB emission in Southeast Asia can reach PRD through long range transport (LRT), resulting in an elevated K^+/EC ratio and MAE_{550}. The Deming regression intercept (11.89) in Figure 8 represents the MAE without the BB effect. This non-BB MAE_{550} (11.89 $m^2\ g^{-1}$) is only slightly lower than $MAE_{p,550}$ (13 $m^2\ g^{-1}$) obtained in section 4.3, implying that a large fraction of $MAE_{p,550}$ could not be explained by the BB source. Additional evidence was obtained through examining regression relationships of $MAE_{p,550}$ with K^+/EC month-by-month (Figure S15b). Correlation of monthly $MAE_{p,550}$ vs. K^+/EC ratio yield a R^2 of 0.23 (Figure S15c). In contrast, a much higher correlation (R^2=0.58) was observed (Figure S15d) between $MAE_{p,550}$ and non-BB MAE_{550} (i.e., K^+/EC intercepts from Figure S15b). These results imply that BB is one of the contributors to the $MAE_{p,550}$ variations, but unlikely the dominating one.

Many studies have found that BB influenced samples exhibit elevated AAE due to the presence of wavelength dependent light absorbing substances like BrC and HUmic-LIke Substances (HULIS) (Kirchstetter et al., 2004; Hoffer et al., 2006; Sandradewi et al., 2008; Herich et al., 2011; Pokhrel et al., 2017). It is of interest to investigate whether elevated AAE observed in the PRD during the dry season is associated with BB influence. As shown in Figure S16, $AAE_{370\text{-}470}$ and $AAE_{470\text{-}660}$ did not correlate with the BB indicator, K^+/EC ratio. These results suggest that the elevated AAE observed in the PRD wintertime is unlikely to be dominated by the BB effect. Beside the independency between $AAE_{470\text{-}660}$ and K^+/EC ratio, the measured $AAE_{470\text{-}660}$ range also implies that BB is not the major driving force of $AAE_{470\text{-}660}$ variations. The limited light absorption contribution from BrC in RPD region is observed in a recent study (Yuan et al., 2016) , which suggest an upper limit of BrC contribution of 10% at 405 nm in the winter time using the AAE approach. As discussed in our Mie simulation (section 3.1) and a previous study (Lack and Cappa, 2010), coating of non-absorbing materials onto soot particles can increase AAE up to 2. Since the monthly average $AAE_{470\text{-}660}$ in wintertime did not exceed 1.2 (Table S3), the variations of $AAE_{470\text{-}660}$ in the PRD are more likely associated with coatings rather than the contribution of BrC. The results also imply that attempts on BrC absorption attribution for the PRD dataset presented in this study could be risky, considering that elevation of AAE is actually dominated by coating (Lack and Langridge, 2013).

4.5 Implications for mixing state

Quantitative direct measurements of BC mixing state and coating thickness are still challenging. SP2 can estimate the coating thickness using a lag-time approach or a Mie calculation approach can be employed, but both methods have a limited range in coating thickness and uncertainties arise from the assumptions made during the retrieval. For example, recent studies found that the mass equivalent diameter of soot core measured by SP2 could be underestimated due to density assumptions (Zhang et al., 2016b). Although size distribution measurement is not available in this study, clues of mixing state still can be derived from bulk measurements of optical properties. As discussed in section 4.4.1, elevated E_{abs550} observed in the rainy season is associated with aged air masses from a marine origin. To probe the possible mixing state difference between dry and rainy season, E_{abs550}, SSA_{525} and

$AAE_{470\text{-}660}$ are used to narrow down the possible core-shell size range as shown in Figure S17. Monthly averages with one standard deviation of $AAE_{470\text{-}660}$, SSA_{525} and E_{abs550} are used as constraints to extract the intersecting core-shell size range from Figure 2a, Figure S4 and Figure 3a. January and August data are used to represent two different scenarios: elevated $AAE_{470\text{-}660}$ (1.19±0.11) with lower E_{abs550} (1.31±0.32) in dry season and low $AAE_{470\text{-}660}$ (1.04±0.09) with elevated E_{abs550} (1.97±0.71) in rainy season. The results show that January and August have a very different core-shell size range: in January, the core and shell range are 100 ~ 160 nm and 120 ~ 250 nm, respectively; in August, the core and shell range are 120 ~ 165 nm and 170 ~ 430 nm, respectively. This confirms again that the soot particles in the rainy season are likely to have a thicker coating than in the dry season.

5 Caveats of the MRS method in its applications to ambient data

5.1 Impact of measurement biases

It should be noted that the E_{abs} estimation approach is insensitive to the systematic MAE bias (e.g. systematic overestimation of σ_{abs} and variability of EC mass by different TOA protocols) discussed in section 2.1, because systematic bias in EC mass or σ_{abs} is cancelled out in the E_{abs} calculation (Eq. 3), since E_{abs} is the ratio of $\sigma_{abs,t}$ to $\sigma_{abs,p}$. To investigate the performance of the MRS approach in response to systematic bias in EC and σ_{abs}, two simple tests are conducted as shown in Figures S18 and S19 by adding systematic biases to the original data. The one-year measurement data of σ_{abs550} and EC are used as original data. Test A represents a situation when σ_{abs} is overestimated and EC is underestimated. The biased data are marked as σ'_{abs550} and EC' respectively, as shown below:

$$\sigma'_{abs550} = \sigma_{abs550} \times 2 \quad (8)$$

$$EC' = EC \times 0.7 \quad (9)$$

As a result, the average MAE_{550} changed from 18.75 to 53.58 $m^2\ g^{-1}$ and MAE_p changed from 13 to 37 $m^2\ g^{-1}$ (Figure S18). However, E_{abs} by ratio of averages remain the same (1.44).

In Test B, EC by different TOA protocols are compared to investigate the effect of different EC determination approaches while σ_{abs550} remains unchanged. EC by IMPROVE TOR protocol is calculated from NIOSH TOT EC following an empirical formula for suburban sites derived from a 3-year OCEC dataset in PRD (Wu et al., 2016a):

$$EC_{IMP\_TOR} = 2.63 \times EC_{NSH\_TOT} + 0.05 \quad (10)$$

As shown in Figure S19, MAE_{550} changed from 18.75 to 7.02 $m^2\ g^{-1}$ and MAE_p changed from 13 to 5 $m^2\ g^{-1}$, but E_{abs} remain almost the same (1.40). Result of Test B implies that although EC is operationally defined, the discrepancy of EC between TOA protocols did not weaken the role of EC serving as a tracer for primary emissions in MRS application. These examples demonstrate that systematic biases in σ_{abs550} and EC have no effects on E_{abs} estimation by the MRS approach.

Study by Cheng et al. (2016) found two distinct types of biomass smoke behave differently on the biases of filter based σ_{abs} measurement. The bias in the first type can be explained by a nearly constant correction factor, which is similar to the situation discussed in Test A. The bias in the second type shows an apparent OC/EC dependence. Test C is carried out to investigate this situation, i.e., examining the impact of sample-dependent bias as a function of E_{abs}. Unlike the proportional bias in Test A and B that is the same for all data points, the bias in Test C depends on the E_{abs550} of individual samples, which are parametrized by Eqs. (11) and (12).

$$\sigma'_{abs550} = \sigma_{abs550} + \sigma_{abs550} \times (k \times E_{abs550} - k) \quad (11)$$

$$EC' = EC - EC \times (k \times E_{abs550} - k) \quad (12)$$

As shown in Eqs. (11) and (12), the positive bias of σ_{abs550} and negative bias of EC are proportional to E_{abs550}. The magnitude of E_{abs550}-dependent bias is regulated by the factor k. Since σ'_{abs550} and EC' are biased in different directions, resulting a further amplification in MAE biases, which could be considered as the extreme case. As shown in Figure S20, for k=10% (corresponding to a bias of 10% when E_{abs}=2), the bias of MRS-derived E_{abs} is very small (1%). For k=20%, the MRS-derived E_{abs} changes from 1.44 to 1.66, leading to a bias of 15%. These results imply that if the measurement bias follows the same form as demonstrated in Test C, the bias is not negligible but still acceptable. If the impact only affects σ_{abs} or EC rather than impacting both, the bias is expected to be smaller than the estimation shown in Test C.

It should be noted that the parameterization scheme shown in Eqs. (11) and (12) is only for demonstration purpose from a conceptual perspective and it does not necessarily represent the real-world measurements. There is a lack of quantitative understanding of this impact. For example, Lee et

al. (2007) used artificially fabricated EC samples with OC coatings to evaluate the impact of coating on OC/EC analysis. Biases were observed, nevertheless, the results were linearly correlated with the true OC and EC values with a high R^2 (>0.9), implying that the biases in that specific study were dominated by systematic biases rather than the coating-dependent bias. Further studies are needed to better characterize and parameterize this impact if filter-based techniques are used for σ_{abs} and EC determination in the MRS approach.

5.2 Impact of semi-volatile organic carbon

Light absorption contribution due to semi-volatile organic carbon (SVOC) from wood combustion was reported to be negligible in the visible range and around 10-20% at 360 nm (Chen and Bond, 2010). On the other hand, OCEC analysis can be affected by SVOC (Subramanian et al., 2004), either by positive artifacts through adsorption of SVOC onto quartz filters, or by negative artifacts through evaporation of SVOC due to the gas-particle re-equilibrium down stream of VOC denuder. Positive artifacts can be minimized by the installation of a VOC denuder which is widely adopted in RT-OCEC measurements (Bae et al., 2004; Bauer et al., 2009). A typical negative artifact of 10% is expected and can be corrected by backup filters (Subramanian et al., 2004). There was evidence to show that SVOC could affect OC/EC split in thermal/optical analysis (Cheng et al., 2009). However, the bias in EC caused by the OC/EC split drift due to SVOC is systematic, making it falls into the scenario discussed in Test B. As a result, the impact from SVOC on E_{abs} estimation by MRS is expected to be small.

5.3 Impact of mineral dust

The presence of mineral dust (MD) could affect both σ_{abs} and EC determination. If MD is externally mixed with soot particles, the light absorption from MD could be miscounted as σ_{abs} enhancement, leading to the overestimation of of E_{abs}. If the light absorption signal from MD is sufficiently strong (e.g. AAE>2), σ_{abs} by MD and BC can be separated by the AAE approach suggested by Fialho et al. (2005). Additionally, the presence of substantial MD in samples has several impacts on the EC determination by thermal analysis. First, if the samples are not pre-treated with acid, the carbonated carbon could be misidentified as EC, resulting over-estimation of EC (Chow et al., 1993). The acid

598 treatment is only available for off-line OC/EC analysis and not yet practical for the RT-OCEC analyzer.
599 Second, metal oxides in MD can lead to premature EC oxidation in the helium stage of OC/EC analysis,
600 leading to underestimation of EC (Wang et al., 2010; Bladt et al., 2012). The lack of a parameterization
601 scheme for correcting the EC loss due to MD makes it improper to use the biased EC as a primary
602 tracer. For these reasons, E_{abs} estimation by MRS is not recommended for samples strongly influenced
603 by MD.

604 5.4 Impact of BrC

605 The data in this study is dominated by BC absorption that did not show much influence from
606 BrC. However, extra care should be taken if the samples exhibit substantial BrC signature (e.g.
607 AAE>2). Such situations are equivalent to the two-source scenarios discussed in our previous paper
608 on the MRS method (Wu and Yu, 2016) and the major findings are described below. Two types of
609 two-source scenarios are considered: two correlated primary sources (scenario A) and two independent
610 primary sources (scenario B). In scenario A in which both BC and primary BrC are dominated by BB,
611 using BC as a solo tracer to calculate the primary ratio (MAE_p) still works. In scenario B in which BC
612 and primary BrC are independent, using BC alone to determine a single primary MAE_p could lead to
613 a considerable bias in E_{abs} estimation. Alternatively, if a reliable primary BrC tracer is available, the
614 corresponding $MAE_{p,BrC}$ can be determined by MRS. With the knowledge of $MAE_{p,BrC}$ and $MAE_{p,BC}$,
615 light absorption by BC and BrC can be calculated separately and the E_{abs} can be determined using Eq.
616 (13) :

617 $$E_{abs} = \frac{\sigma_{abs,t}}{\sigma_{abs,p,BC}+\sigma_{abs,p,BrC}} = \frac{\sigma_{abs,t}}{MAE_{p,BC}\times EC+MAE_{p,BrC}\times BrC} \quad (13)$$

618 However, the implementation of Eq.13 is challenging due to the complexity in the chemical
619 composition of BrC. For example, a recent study found that the 20 most absorbing BrC chromophores
620 account for ~50% BrC light absorption and there is not a single compound contributing more than 10%
621 (Lin et al., 2016), making it difficult to choose a single compound as the BrC tracer. In addition, time
622 resolved measurement of BrC chromophores has yet to emerge. As a result, for scenario B (sample
623 AAE>2 & primary BrC variations independent of BC), estimation of E_{abs} by MRS is not practical at

this stage due to the lack of required input data. Using BC alone to determine a single primary MAE_p could lead to a considerable bias and should be avoided.

6 Conclusions

In this study, a novel statistical approach is proposed and its application on ambient data is demonstrated using one-year hourly OC and EC data coupled with Aethalometer measurements. Unlike conventional E_{abs} determination approaches that require expensive instrumentation (e.g. TD-PAS, VTDMA, SP2), this new approach employs widely deployed instruments (field carbon analyzer and Aethalometer). The key of this new approach involves calculating MAE_p by the Minimum R Squared (MRS) method (Wu and Yu, 2016). The MRS method opens up a new approach to investigate the long-term trend of E_{abs} that was rarely studied by the TD approach. It is found that E_{abs} estimation by MRS is insensitive to systematic biases in EC and σ_{abs} measurements. The annual average $MAE_{p,550}$ estimated by MRS is 13 $m^2 g^{-1}$ and annual average MAE_{550} is 18.75±6.16 $m^2 g^{-1}$, suggesting an annual average enhancement factor (E_{abs550}) of 1.50±0.48 in the PRD region. This value is within the upper limit of E_{abs} (~2) by core-shell Mie simulations considering the typical soot size distribution and coating thickness in the PRD.

Both $MAE_{p,550}$ and E_{abs} show distinct seasonal variations, implying the complexity of soot particle mixing state variations in this region. The elevated summertime E_{abs550} in the PRD is found to be associated with the domination of aged air masses from the South China Sea, along with the long-range transport of biomass burning influenced air masses from Southeast Asia. Core-shell size ranges narrowed down by E_{abs550} and $AAE_{470\text{-}660}$ constraints suggest that soot particles in the rainy season are likely to have thicker coatings than in the dry season.

Data availability

OC, EC, inorganic ions and σ_{abs} data used in this study are available from corresponding authors upon request.

Acknowledgements

This work is supported by the National Natural Science Foundation of China (41605002, 41475004). We gratefully acknowledge the Fok Ying Tung Foundation for funding to the Atmospheric Research Center at HKUST Fok Ying Tung Graduate School. The authors thank Jingxiang Huang of Fok Ying Tung Graduate School for the assistance in OCEC analyzer maintenance. The authors are also grateful to Dr. Stephen M Griffith and Dr. Yongjie Li for the helpful comments. The authors gratefully acknowledge the NOAA Air Resources Laboratory (ARL) for the provision of the HYSPLIT transport and dispersion model used in this publication.

References

Adler, G., Riziq, A. A., Erlick, C., and Rudich, Y.: Effect of intrinsic organic carbon on the optical properties of fresh diesel soot, Proceedings of the National Academy of Sciences, 107, 6699-6704, doi: 10.1073/pnas.0903311106, 2010.

Ajtai, T., Filep, Á., Utry, N., Schnaiter, M., Linke, C., Bozóki, Z., Szabó, G., and Leisner, T.: Inter-comparison of optical absorption coefficients of atmospheric aerosols determined by a multi-wavelength photoacoustic spectrometer and an Aethalometer under sub-urban wintry conditions, J. Aerosol. Sci., 42, 859-866, doi: 10.1016/j.jaerosci.2011.07.008, 2011.

Alexander, D. T. L., Crozier, P. A., and Anderson, J. R.: Brown carbon spheres in East Asian outflow and their optical properties, Science, 321, 833-836, 2008.

Andreae, M. O., Schmid, O., Yang, H., Chand, D., Yu, J. Z., Zeng, L. M., and Zhang, Y. H.: Optical properties and chemical composition of the atmospheric aerosol in urban Guangzhou, China, Atmos. Environ., 42, 6335-6350, doi: 10.1016/j.atmosenv.2008.01.030, 2008.

Aouizerats, B., van der Werf, G. R., Balasubramanian, R., and Betha, R.: Importance of transboundary transport of biomass burning emissions to regional air quality in Southeast Asia during a high fire event, Atmos. Chem. Phys., 15, 363-373, doi: 10.5194/acp-15-363-2015, 2015.

Arnott, W. P., Moosmuller, H., Sheridan, P. J., Ogren, J. A., Raspet, R., Slaton, W. V., Hand, J. L., Kreidenweis, S. M., and Collett, J. L.: Photoacoustic and filter-based ambient aerosol light absorption measurements: Instrument comparisons and the role of relative humidity, J. Geophys. Res., 108, 2003.

Arnott, W. P., Hamasha, K., Moosmuller, H., Sheridan, P. J., and Ogren, J. A.: Towards aerosol light-absorption measurements with a 7-wavelength Aethalometer: Evaluation with a photoacoustic instrument and 3-wavelength nephelometer, Aerosol. Sci. Technol., 39, 17-29, doi: 10.1080/027868290901972, 2005.

Bae, M. S., Schauer, J. J., DeMinter, J. T., Turner, J. R., Smith, D., and Cary, R. A.: Validation of a semi-continuous instrument for elemental carbon and organic carbon using a thermal-optical method, Atmos. Environ., 38, 2885-2893, doi: 10.1016/j.atmosenv.2004.02.027, 2004.

Bauer, J. J., Yu, X.-Y., Cary, R., Laulainen, N., and Berkowitz, C.: Characterization of the sunset semi-continuous carbon aerosol analyzer, J. Air Waste Manage. Assoc., 59, 826-833, doi: 10.3155/1047-3289.59.7.826, 2009.

Bladt, H., Schmid, J., Kireeva, E. D., Popovicheva, O. B., Perseantseva, N. M., Timofeev, M. A., Heister, K., Uihlein, J., Ivleva, N. P., and Niessner, R.: Impact of Fe Content in Laboratory-Produced Soot Aerosol on its Composition, Structure, and Thermo-Chemical Properties, Aerosol. Sci. Technol., 46, 1337-1348, doi: 10.1080/02786826.2012.711917, 2012.

Bohren, C. F. and Huffman, D. R.: Absorption and scattering of light by small particles, Wiley, New York, xiv, 530 p. pp., 1983.

Bond, T. C.: Spectral dependence of visible light absorption by carbonaceous particles emitted from coal combustion, Geophys. Res. Lett., 28, 4075-4078, doi: 10.1029/2001gl013652, 2001.

Bond, T. C. and Bergstrom, R. W.: Light absorption by carbonaceous particles: An investigative review, Aerosol. Sci. Technol., 40, 27-67, doi: 10.1080/02786820500421521, 2006.

Bond, T. C., Habib, G., and Bergstrom, R. W.: Limitations in the enhancement of visible light absorption due to mixing state, J. Geophys. Res., 111, -, doi: 10.1029/2006JD007315, 2006.

Bond, T. C., Zarzycki, C., Flanner, M. G., and Koch, D. M.: Quantifying immediate radiative forcing by black carbon and organic matter with the Specific Forcing Pulse, Atmos. Chem. Phys., 11, 1505-1525, doi: 10.5194/acp-11-1505-2011, 2011.

Cappa, C. D., Lack, D. A., Burkholder, J. B., and Ravishankara, A. R.: Bias in Filter-Based Aerosol Light Absorption Measurements Due to Organic Aerosol Loading: Evidence from Laboratory Measurements, Aerosol. Sci. Technol., 42, 1022-1032, doi: 10.1080/02786820802389285, 2008.

Cappa, C. D., Onasch, T. B., Massoli, P., Worsnop, D. R., Bates, T. S., Cross, E. S., Davidovits, P., Hakala, J., Hayden, K. L., Jobson, B. T., Kolesar, K. R., Lack, D. A., Lerner, B. M., Li, S.-M., Mellon, D., Nuaaman, I., Olfert, J. S., Petäjä, T., Quinn, P. K., Song, C., Subramanian, R., Williams, E. J., and Zaveri, R. A.: Radiative Absorption Enhancements Due to the Mixing State of Atmospheric Black Carbon, Science, 337, 1078-1081, doi: 10.1126/science.1223447, 2012.

Chan, T. W., Brook, J. R., Smallwood, G. J., and Lu, G.: Time-resolved measurements of black carbon light absorption enhancement in urban and near-urban locations of southern Ontario, Canada, Atmos. Chem. Phys., 11, 10407-10432, doi: 10.5194/acp-11-10407-2011, 2011.

Chen, B., Bai, Z., Cui, X., Chen, J., Andersson, A., and Gustafsson, Ö.: Light absorption enhancement of black carbon from urban haze in Northern China winter, Environ Pollut, 221, 418-426, doi: 10.1016/j.envpol.2016.12.004, 2017.

Chen, Y. and Bond, T. C.: Light absorption by organic carbon from wood combustion, Atmos. Chem. Phys., 10, 1773-1787, doi: 10.5194/acp-10-1773-2010, 2010.

Cheng, Y., He, K. B., Duan, F. K., Zheng, M., Ma, Y. L., and Tan, J. H.: Positive sampling artifact of carbonaceous aerosols and its influence on the thermal-optical split of OC/EC, Atmos. Chem. Phys., 9, 7243-7256, doi: 10.5194/acp-9-7243-2009, 2009.

Cheng, Y., Engling, G., Moosmüller, H., Arnott, W. P., Chen, L. W. A., Wold, C. E., Hao, W. M., and He, K.-b.: Light absorption by biomass burning source emissions, Atmos. Environ., 127, 347-354, doi: 10.1016/j.atmosenv.2015.12.045, 2016.

China, S., Mazzoleni, C., Gorkowski, K., Aiken, A. C., and Dubey, M. K.: Morphology and mixing state of individual freshly emitted wildfire carbonaceous particles, Nat Commun, 4, doi: 10.1038/ncomms3122, 2013.

Chow, J. C., Watson, J. G., Pritchett, L. C., Pierson, W. R., Frazier, C. A., and Purcell, R. G.: The DRI thermal/optical reflectance carbon analysis system: description, evaluation and applications in United-States air-quality studies, Atmos. Environ., 27, 1185-1201, doi: 10.1016/0960-1686(93)90245-T, 1993.

Chow, J. C., Watson, J. G., Doraiswamy, P., Chen, L. W. A., Sodeman, D. A., Lowenthal, D. H., Park, K., Arnott, W. P., and Motallebi, N.: Aerosol light absorption, black carbon, and elemental carbon at the Fresno Supersite, California, Atmos Res, 93, 874-887, doi: 10.1016/j.atmosres.2009.04.010, 2009.

Coen, M. C., Weingartner, E., Apituley, A., Ceburnis, D., Fierz-Schmidhauser, R., Flentje, H., Henzing, J. S., Jennings, S. G., Moerman, M., Petzold, A., Schmid, O., and Baltensperger, U.: Minimizing light absorption measurement artifacts of the Aethalometer: evaluation of five correction algorithms, Atmos. Meas. Tech., 3, 457-474, doi: 10.5194/amt-3-457-2010, 2010.

Cui, F., Chen, M., Ma, Y., Zheng, J., Zhou, Y., Li, S., Qi, L., and Wang, L.: An intensive study on aerosol optical properties and affecting factors in Nanjing, China, Journal of Environmental Sciences, 40, 35-43, doi: 10.1016/j.jes.2015.08.017, 2016a.

741 Cui, X., Wang, X., Yang, L., Chen, B., Chen, J., Andersson, A., and Gustafsson, Ö.: Radiative
742 absorption enhancement from coatings on black carbon aerosols, Sci.Total.Environ., 551, 51-56, doi:
743 10.1016/j.scitotenv.2016.02.026, 2016b.
744 Dastanpour, R., Momenimovahed, A., Thomson, K., Olfert, J., and Rogak, S.: Variation of the optical
745 properties of soot as a function of particle mass, Carbon, 124, 201-211, doi:
746 10.1016/j.carbon.2017.07.005, 2017.
747 Ding, A. J., Huang, X., Nie, W., Sun, J. N., Kerminen, V. M., Petäjä, T., Su, H., Cheng, Y. F., Yang,
748 X. Q., Wang, M. H., Chi, X. G., Wang, J. P., Virkkula, A., Guo, W. D., Yuan, J., Wang, S. Y., Zhang,
749 R. J., Wu, Y. F., Song, Y., Zhu, T., Zilitinkevich, S., Kulmala, M., and Fu, C. B.: Enhanced haze
750 pollution by black carbon in megacities in China, Geophys. Res. Lett., 43, 2873-2879, doi:
751 10.1002/2016GL067745, 2016.
752 Doran, J. C., Barnard, J. C., Arnott, W. P., Cary, R., Coulter, R., Fast, J. D., Kassianov, E. I., Kleinman,
753 L., Laulainen, N. S., Martin, T., Paredes-Miranda, G., Pekour, M. S., Shaw, W. J., Smith, D. F.,
754 Springston, S. R., and Yu, X. Y.: The T1-T2 study: evolution of aerosol properties downwind of
755 Mexico City, Atmos. Chem. Phys., 7, 1585-1598, doi: 10.5194/acp-7-1585-2007, 2007.
756 Draxier, R. R. and Hess, G. D.: An overview of the HYSPLIT_4 modelling system for trajectories,
757 dispersion and deposition, Aust Meteorol Mag, 47, 295-308, 1998.
758 Drinovec, L., Gregorič, A., Zotter, P., Wolf, R., Bruns, E. A., Prévôt, A. S. H., Petit, J. E., Favez, O.,
759 Sciare, J., Arnold, I. J., Chakrabarty, R. K., Moosmüller, H., Filep, A., and Močnik, G.: The filter-
760 loading effect by ambient aerosols in filter absorption photometers depends on the coating of the
761 sampled particles, Atmos. Meas. Tech., 10, 1043-1059, doi: 10.5194/amt-10-1043-2017, 2017.
762 Fialho, P., Hansen, A. D. A., and Honrath, R. E.: Absorption coefficients by aerosols in remote areas:
763 a new approach to decouple dust and black carbon absorption coefficients using seven-wavelength
764 Aethalometer data, J. Aerosol. Sci., 36, 267-282, doi: 10.1016/j.jaerosci.2004.09.004, 2005.
765 Fuller, K. A., Malm, W. C., and Kreidenweis, S. M.: Effects of mixing on extinction by carbonaceous
766 particles, J. Geophys. Res., 104, 15941-15954, 1999.
767 Gong, X., Zhang, C., Chen, H., Nizkorodov, S. A., Chen, J., and Yang, X.: Size distribution and mixing
768 state of black carbon particles during a heavy air pollution episode in Shanghai, Atmos. Chem. Phys.,
769 16, 5399-5411, doi: 10.5194/acp-16-5399-2016, 2016.
770 Guo, S., Hu, M., Lin, Y., Gomez-Hernandez, M., Zamora, M. L., Peng, J., Collins, D. R., and Zhang,
771 R.: OH-Initiated Oxidation of m-Xylene on Black Carbon Aging, Environ. Sci. Technol., doi:
772 10.1021/acs.est.6b01272, 2016.
773 Guyon, P., Graham, B., Roberts, G. C., Mayol-Bracero, O. L., Maenhaut, W., Artaxo, P., and Andreae,
774 M. O.: Sources of optically active aerosol particles over the Amazon forest, Atmos. Environ., 38, 1039-
775 1051, doi: 10.1016/j.atmosenv.2003.10.051, 2004.
776 Hansen, A. D. A.: The Aethalometer Manual, Berkeley, California,USA, Magee Scientific, 2005.
777 Hansen, J. and Nazarenko, L.: Soot climate forcing via snow and ice albedos, P Natl Acad Sci USA,
778 101, 423-428, doi: 10.1073/pnas.2237157100, 2004.
779 Healy, R. M., Wang, J. M., Jeong, C. H., Lee, A. K. Y., Willis, M. D., Jaroudi, E., Zimmerman, N.,
780 Hilker, N., Murphy, M., Eckhardt, S., Stohl, A., Abbatt, J. P. D., Wenger, J. C., and Evans, G. J.: Light-
781 absorbing properties of ambient black carbon and brown carbon from fossil fuel and biomass burning
782 sources, J. Geophys. Res., 120, 2015JD023382, doi: 10.1002/2015JD023382, 2015.

783 Herich, H., Hueglin, C., and Buchmann, B.: A 2.5 year's source apportionment study of black carbon
784 from wood burning and fossil fuel combustion at urban and rural sites in Switzerland, Atmos. Meas.
785 Tech., 4, 1409-1420, doi: 10.5194/amt-4-1409-2011, 2011.
786 Hoffer, A., Gelencser, A., Guyon, P., Kiss, G., Schmid, O., Frank, G. P., Artaxo, P., and Andreae, M.
787 O.: Optical properties of humic-like substances (HULIS) in biomass-burning aerosols, Atmos. Chem.
788 Phys., 6, 3563-3570, 2006.
789 Huang, X. F., He, L. Y., Hu, M., Canagaratna, M. R., Kroll, J. H., Ng, N. L., Zhang, Y. H., Lin, Y.,
790 Xue, L., Sun, T. L., Liu, X. G., Shao, M., Jayne, J. T., and Worsnop, D. R.: Characterization of
791 submicron aerosols at a rural site in Pearl River Delta of China using an Aerodyne High-Resolution
792 Aerosol Mass Spectrometer, Atmos. Chem. Phys., 11, 1865-1877, doi: 10.5194/acp-11-1865-2011,
793 2011.
794 IPCC: Climate change 2013 : the physical science basis : Working Group I contribution to the Fifth
795 Assessment Report of the Intergovernmental Panel on Climate Change, xi, 1535 pages. pp., 2013.
796 Jacobson, M. Z.: Effects of externally-through-internally-mixed soot inclusions within clouds and
797 precipitation on global climate, J Phys Chem A, 110, 6860-6873, doi: 10.1021/jp056391r, 2006.
798 Jason Blake, C.: Quantifying the occurrence and magnitude of the Southeast Asian fire climatology,
799 Environmental Research Letters, 9, 114018, 2014.
800 Jung, J., Lee, H., Kim, Y. J., Liu, X., Zhang, Y., Gu, J., and Fan, S.: Aerosol chemistry and the effect
801 of aerosol water content on visibility impairment and radiative forcing in Guangzhou during the 2006
802 Pearl River Delta campaign, Journal of Environmental Management, 90, 3231-3244, doi:
803 10.1016/j.jenvman.2009.04.021, 2009.
804 Khalizov, A. F., Xue, H. X., Wang, L., Zheng, J., and Zhang, R. Y.: Enhanced Light Absorption and
805 Scattering by Carbon Soot Aerosol Internally Mixed with Sulfuric Acid, J Phys Chem A, 113, 1066-
806 1074, doi: 10.1021/jp807531n, 2009.
807 Kirchstetter, T. W., Novakov, T., and Hobbs, P. V.: Evidence that the spectral dependence of light
808 absorption by aerosols is affected by organic carbon, J. Geophys. Res., 109, D21208, doi:
809 10.1029/2004jd004999, 2004.
810 Knox, A., Evans, G. J., Brook, J. R., Yao, X., Jeong, C. H., Godri, K. J., Sabaliauskas, K., and Slowik,
811 J. G.: Mass Absorption Cross-Section of Ambient Black Carbon Aerosol in Relation to Chemical Age,
812 Aerosol. Sci. Technol., 43, 522-532, doi: 10.1080/02786820902777207, 2009.
813 Koch, D. and Del Genio, A.: Black carbon semi-direct effects on cloud cover: review and synthesis,
814 Atmos. Chem. Phys., 10, 7685-7696, 2010.
815 Kozlov, V. S., Panchenko, M. V., Tikhomirov, A. B., Tikhomirov, B. A., and Shmargunov, V. P.:
816 Effect of relative air humidity on photoacoustic aerosol absorption measurements in the near-ground
817 atmospheric layer, Atmospheric and Oceanic Optics, 24, 487, doi: 10.1134/s1024856011050101, 2011.
818 Laborde, M., Mertes, P., Zieger, P., Dommen, J., Baltensperger, U., and Gysel, M.: Sensitivity of the
819 Single Particle Soot Photometer to different black carbon types, Atmos. Meas. Tech., 5, 1031-1043,
820 doi: 10.5194/amt-5-1031-2012, 2012.
821 Lack, D. A. and Cappa, C. D.: Impact of brown and clear carbon on light absorption enhancement,
822 single scatter albedo and absorption wavelength dependence of black carbon, Atmos. Chem. Phys., 10,
823 4207-4220, doi: 10.5194/acp-10-4207-2010, 2010.

Lack, D. A., Langridge, J. M., Bahreini, R., Cappa, C. D., Middlebrook, A. M., and Schwarz, J. P.: Brown carbon and internal mixing in biomass burning particles, P Natl Acad Sci USA, 109, 14802-14807, doi: 10.1073/pnas.1206575109, 2012a.
Lack, D. A., Richardson, M. S., Law, D., Langridge, J. M., Cappa, C. D., McLaughlin, R. J., and Murphy, D. M.: Aircraft instrument for comprehensive characterization of aerosol optical properties, Part 2: black and brown carbon absorption and absorption enhancement measured with photo acoustic spectroscopy, Aerosol. Sci. Technol., 46, 555-568, doi: 10.1080/02786826.2011.645955, 2012b.
Lack, D. A. and Langridge, J. M.: On the attribution of black and brown carbon light absorption using the Ångström exponent, Atmos. Chem. Phys., 13, 10535-10543, doi: 10.5194/acp-13-10535-2013, 2013.
Lan, Z.-J., Huang, X.-F., Yu, K.-Y., Sun, T.-L., Zeng, L.-W., and Hu, M.: Light absorption of black carbon aerosol and its enhancement by mixing state in an urban atmosphere in South China, Atmos. Environ., 69, 118-123, doi: 10.1016/j.atmosenv.2012.12.009, 2013.
Langridge, J. M., Richardson, M. S., Lack, D. A., Brock, C. A., and Murphy, D. M.: Limitations of the Photoacoustic Technique for Aerosol Absorption Measurement at High Relative Humidity, Aerosol. Sci. Technol., 47, 1163-1173, doi: 10.1080/02786826.2013.827324, 2013.
Lee, H. M., Okuyama, K., Mizohata, A., Kim, T. O., and Koyama, H.: Fabrication of reference filter for measurements of EC (elemental carbon) and OC (organic carbon) in aerosol particles, Aerosol. Sci. Technol., 41, 284-294, doi: 10.1080/02786820701197060, 2007.
Leung, K. K., Schnitzler, E. G., Jäger, W., and Olfert, J. S.: Relative Humidity Dependence of Soot Aggregate Restructuring Induced by Secondary Organic Aerosol: Effects of Water on Coating Viscosity and Surface Tension, Environmental Science & Technology Letters, doi: 10.1021/acs.estlett.7b00298, 2017.
Lewis, K. A., Arnott, W. P., Moosmuller, H., Chakrabarty, R. K., Carrico, C. M., Kreidenweis, S. M., Day, D. E., Malm, W. C., Laskin, A., Jimenez, J. L., Ulbrich, I. M., Huffman, J. A., Onasch, T. B., Trimborn, A., Liu, L., and Mishchenko, M. I.: Reduction in biomass burning aerosol light absorption upon humidification: roles of inorganically-induced hygroscopicity, particle collapse, and photoacoustic heat and mass transfer, Atmos. Chem. Phys., 9, 8949-8966, doi: 10.5194/acp-9-8949-2009, 2009a.
Lewis, K. A., Arnott, W. P., Moosmüller, H., Chakrabarty, R. K., Carrico, C. M., Kreidenweis, S. M., Day, D. E., Malm, W. C., Laskin, A., Jimenez, J. L., Ulbrich, I. M., Huffman, J. A., Onasch, T. B., Trimborn, A., Liu, L., and Mishchenko, M. I.: Reduction in biomass burning aerosol light absorption upon humidification: roles of inorganically-induced hygroscopicity, particle collapse, and photoacoustic heat and mass transfer, Atmos. Chem. Phys., 9, 8949-8966, doi: 10.5194/acp-9-8949-2009, 2009b.
Lin, P., Aiona, P. K., Li, Y., Shiraiwa, M., Laskin, J., Nizkorodov, S. A., and Laskin, A.: Molecular Characterization of Brown Carbon in Biomass Burning Aerosol Particles, Environ. Sci. Technol., 50, 11815-11824, doi: 10.1021/acs.est.6b03024, 2016.
Liu, D., Whitehead, J., Alfarra, M. R., Reyes-Villegas, E., Spracklen, D. V., Reddington, C. L., Kong, S., Williams, P. I., Ting, Y.-C., Haslett, S., Taylor, J. W., Flynn, M. J., Morgan, W. T., McFiggans, G., Coe, H., and Allan, J. D.: Black-carbon absorption enhancement in the atmosphere determined by particle mixing state, Nature Geosci, 10, 184-188, doi: 10.1038/ngeo2901, 2017.

Liu, F., Yon, J., and Bescond, A.: On the radiative properties of soot aggregates – Part 2: Effects of coating, Journal of Quantitative Spectroscopy and Radiative Transfer, 172, 134-145, doi: 10.1016/j.jqsrt.2015.08.005, 2016a.

Liu, J., Lin, P., Laskin, A., Laskin, J., Kathmann, S. M., Wise, M., Caylor, R., Imholt, F., Selimovic, V., and Shilling, J. E.: Optical properties and aging of light-absorbing secondary organic aerosol, Atmos. Chem. Phys., 16, 12815-12827, doi: 10.5194/acp-16-12815-2016, 2016b.

Liu, S., Aiken, A. C., Gorkowski, K., Dubey, M. K., Cappa, C. D., Williams, L. R., Herndon, S. C., Massoli, P., Fortner, E. C., Chhabra, P. S., Brooks, W. A., Onasch, T. B., Jayne, J. T., Worsnop, D. R., China, S., Sharma, N., Mazzoleni, C., Xu, L., Ng, N. L., Liu, D., Allan, J. D., Lee, J. D., Fleming, Z. L., Mohr, C., Zotter, P., Szidat, S., and Prevot, A. S. H.: Enhanced light absorption by mixed source black and brown carbon particles in UK winter, Nat Commun, 6, doi: 10.1038/ncomms9435, 2015.

Ma, N., Zhao, C. S., Muller, T., Cheng, Y. F., Liu, P. F., Deng, Z. Z., Xu, W. Y., Ran, L., Nekat, B., van Pinxteren, D., Gnauk, T., Mueller, K., Herrmann, H., Yan, P., Zhou, X. J., and Wiedensohler, A.: A new method to determine the mixing state of light absorbing carbonaceous using the measured aerosol optical properties and number size distributions, Atmos. Chem. Phys., 12, 2381-2397, doi: 10.5194/acp-12-2381-2012, 2012.

Replacement Filter Tape for the Magee Scientific Model AE33 Aethalometer®: http://www.mageesci.com/images/stories/docs/Magee_Scientific_Filter_Aethalometer_AE_Tape_Replacement_discussion.pdf, 2017.

Matsui, H., Koike, M., Kondo, Y., Moteki, N., Fast, J. D., and Zaveri, R. A.: Development and validation of a black carbon mixing state resolved three-dimensional model: Aging processes and radiative impact, J. Geophys. Res., 118, 2304-2326, doi: 10.1029/2012JD018446, 2013.

McMeeking, G. R., Fortner, E., Onasch, T. B., Taylor, J. W., Flynn, M., Coe, H., and Kreidenweis, S. M.: Impacts of nonrefractory material on light absorption by aerosols emitted from biomass burning, J. Geophys. Res., 119, 12,272-212,286, doi: 10.1002/2014JD021750, 2014.

Moffet, R. C., O'Brien, R. E., Alpert, P. A., Kelly, S. T., Pham, D. Q., Gilles, M. K., Knopf, D. A., and Laskin, A.: Morphology and mixing of black carbon particles collected in central California during the CARES field study, Atmos. Chem. Phys., 16, 14515-14525, doi: 10.5194/acp-16-14515-2016, 2016.

Moosmuller, H., Chakrabarty, R. K., Ehlers, K. M., and Arnott, W. P.: Absorption Angstrom coefficient, brown carbon, and aerosols: basic concepts, bulk matter, and spherical particles, Atmos. Chem. Phys., 11, 1217-1225, doi: 10.5194/acp-11-1217-2011, 2011.

Moteki, N., Kondo, Y., and Adachi, K.: Identification by single-particle soot photometer of black carbon particles attached to other particles: Laboratory experiments and ground observations in Tokyo, J. Geophys. Res., 119, 2013JD020655, doi: 10.1002/2013jd020655, 2014.

Nakayama, T., Ikeda, Y., Sawada, Y., Setoguchi, Y., Ogawa, S., Kawana, K., Mochida, M., Ikemori, F., Matsumoto, K., and Matsumi, Y.: Properties of light-absorbing aerosols in the Nagoya urban area, Japan, in August 2011 and January 2012: Contributions of brown carbon and lensing effect, J. Geophys. Res., 119, 2014JD021744, doi: 10.1002/2014JD021744, 2014.

Naoe, H., Hasegawa, S., Heintzenberg, J., Okada, K., Uchiyama, A., Zaizen, Y., Kobayashi, E., and Yamazaki, A.: State of mixture of atmospheric submicrometer black carbon particles and its effect on particulate light absorption, Atmos. Environ., 43, 1296-1301, doi: 10.1016/j.atmosenv.2008.11.031, 2009.

908 Nordmann, S., Cheng, Y. F., Carmichael, G. R., Yu, M., Denier van der Gon, H. A. C., Zhang, Q.,
909 Saide, P. E., Pöschl, U., Su, H., Birmili, W., and Wiedensohler, A.: Atmospheric black carbon and
910 warming effects influenced by the source and absorption enhancement in central Europe, Atmos. Chem.
911 Phys., 14, 12683-12699, doi: 10.5194/acp-14-12683-2014, 2014.
912 Pandey, A., Pervez, S., and Chakrabarty, R. K.: Filter-based measurements of UV–vis mass absorption
913 cross sections of organic carbon aerosol from residential biomass combustion: Preliminary findings
914 and sources of uncertainty, Journal of Quantitative Spectroscopy and Radiative Transfer, 182, 296-
915 304, doi: 10.1016/j.jqsrt.2016.06.023, 2016.
916 Pei, X., Hallquist, M., Eriksson, A. C., Pagels, J. H., Donahue, N. M., Mentel, T., Svenningsson, B.,
917 Brune, W., and Pathak, R. K.: Morphological transformation of soot: investigation of microphysical
918 processes during the condensation of sulfuric acid and limonene ozonolysis product vapors, Atmos.
919 Chem. Phys. Discuss., 2017, 1-30, doi: 10.5194/acp-2017-769, 2017.
920 Peng, J., Hu, M., Guo, S., Du, Z., Zheng, J., Shang, D., Levy Zamora, M., Zeng, L., Shao, M., Wu, Y.-
921 S., Zheng, J., Wang, Y., Glen, C. R., Collins, D. R., Molina, M. J., and Zhang, R.: Markedly enhanced
922 absorption and direct radiative forcing of black carbon under polluted urban environments,
923 Proceedings of the National Academy of Sciences, 113, 4266-4271, doi: 10.1073/pnas.1602310113,
924 2016.
925 Pokhrel, R. P., Beamesderfer, E. R., Wagner, N. L., Langridge, J. M., Lack, D. A., Jayarathne, T.,
926 Stone, E. A., Stockwell, C. E., Yokelson, R. J., and Murphy, S. M.: Relative importance of black
927 carbon, brown carbon, and absorption enhancement from clear coatings in biomass burning emissions,
928 Atmos. Chem. Phys., 17, 5063-5078, doi: 10.5194/acp-17-5063-2017, 2017.
929 Ramanathan, V. and Carmichael, G.: Global and regional climate changes due to black carbon, Nat
930 Geosci, 1, 221-227, doi: 10.1038/Ngeo156, 2008.
931 Raspet, R., Slaton, W. V., Arnott, W. P., and Moosmüller, H.: Evaporation–Condensation Effects on
932 Resonant Photoacoustics of Volatile Aerosols, Journal of Atmospheric and Oceanic Technology, 20,
933 685-695, doi: 10.1175/1520-0426(2003)20<685:eceorp>2.0.co;2, 2003.
934 Reid, J. S., Eck, T. F., Christopher, S. A., Koppmann, R., Dubovik, O., Eleuterio, D. P., Holben, B. N.,
935 Reid, E. A., and Zhang, J.: A review of biomass burning emissions part III: intensive optical properties
936 of biomass burning particles, Atmos. Chem. Phys., 5, 827-849, doi: 10.5194/acp-5-827-2005, 2005.
937 Roden, C. A., Bond, T. C., Conway, S., and Pinel, A. B. O.: Emission factors and real-time optical
938 properties of particles emitted from traditional wood burning cookstoves, Environ. Sci. Technol., 40,
939 6750-6757, doi: 10.1021/es052080i, 2006.
940 Rose, D., Wehner, B., Ketzel, M., Engler, C., Voigtländer, J., Tuch, T., and Wiedensohler, A.:
941 Atmospheric number size distributions of soot particles and estimation of emission factors, Atmos.
942 Chem. Phys., 6, 1021-1031, doi: 10.5194/acp-6-1021-2006, 2006.
943 Saathoff, H., Naumann, K. H., Schnaiter, M., Schöck, W., Möhler, O., Schurath, U., Weingartner, E.,
944 Gysel, M., and Baltensperger, U.: Coating of soot and (NH4)2SO4 particles by ozonolysis products of
945 α-pinene, J. Aerosol. Sci., 34, 1297-1321, doi: 10.1016/S0021-8502(03)00364-1, 2003.
946 Sandradewi, J., Prévôt, A. S. H., Weingartner, E., Schmidhauser, R., Gysel, M., and Baltensperger, U.:
947 A study of wood burning and traffic aerosols in an Alpine valley using a multi-wavelength
948 Aethalometer, Atmos. Environ., 42, 101-112, doi: 10.1016/j.atmosenv.2007.09.034, 2008.

949 Saturno, J., Pöhlker, C., Massabò, D., Brito, J., Carbone, S., Cheng, Y., Chi, X., Ditas, F., Hrabě de
950 Angelis, I., Morán-Zuloaga, D., Pöhlker, M. L., Rizzo, L. V., Walter, D., Wang, Q., Artaxo, P., Prati,
951 P., and Andreae, M. O.: Comparison of different Aethalometer correction schemes and a reference
952 multi-wavelength absorption technique for ambient aerosol data, Atmos. Meas. Tech., 10, 2837-2850,
953 doi: 10.5194/amt-10-2837-2017, 2017.
954 Schmid, O., Artaxo, P., Arnott, W. P., Chand, D., Gatti, L. V., Frank, G. P., Hoffer, A., Schnaiter, M.,
955 and Andreae, M. O.: Spectral light absorption by ambient aerosols influenced by biomass burning in
956 the Amazon Basin. I: Comparison and field calibration of absorption measurement techniques, Atmos.
957 Chem. Phys., 6, 3443-3462, doi: 10.5194/acp-6-3443-2006, 2006.
958 Schnaiter, M., Linke, C., Mohler, O., Naumann, K. H., Saathoff, H., Wagner, R., Schurath, U., and
959 Wehner, B.: Absorption amplification of black carbon internally mixed with secondary organic aerosol,
960 J. Geophys. Res., 110, doi: 10.1029/2005JD006046, 2005.
961 Schwarz, J. P., Spackman, J. R., Fahey, D. W., Gao, R. S., Lohmann, U., Stier, P., Watts, L. A.,
962 Thomson, D. S., Lack, D. A., Pfister, L., Mahoney, M. J., Baumgardner, D., Wilson, J. C., and Reeves,
963 J. M.: Coatings and their enhancement of black carbon light absorption in the tropical atmosphere, J.
964 Geophys. Res., 113, -, doi: 10.1029/2007JD009042, 2008.
965 Sedlacek, A. J., Lewis, E. R., Kleinman, L., Xu, J. Z., and Zhang, Q.: Determination of and evidence
966 for non-core-shell structure of particles containing black carbon using the Single-Particle Soot
967 Photometer (SP2), Geophys. Res. Lett., 39, doi: 10.1029/2012GL050905, 2012.
968 Shen, G., Chen, Y., Wei, S., Fu, X., Zhu, Y., and Tao, S.: Mass absorption efficiency of elemental
969 carbon for source samples from residential biomass and coal combustions, Atmos. Environ., 79, 79-
970 84, doi: 10.1016/j.atmosenv.2013.05.082, 2013.
971 Shiraiwa, M., Kondo, Y., Iwamoto, T., and Kita, K.: Amplification of Light Absorption of Black
972 Carbon by Organic Coating, Aerosol. Sci. Technol., 44, 46-54, doi: 10.1080/02786820903357686,
973 2010.
974 Subramanian, R., Khlystov, A. Y., Cabada, J. C., and Robinson, A. L.: Positive and negative artifacts
975 in particulate organic carbon measurements with denuded and undenuded sampler configurations,
976 Aerosol. Sci. Technol., 38, 27-48, doi: 10.1080/02786820390229354, 2004.
977 Suglia, S. F., Gryparis, A., Wright, R. O., Schwartz, J., and Wright, R. J.: Association of Black Carbon
978 with Cognition among Children in a Prospective Birth Cohort Study, American Journal of
979 Epidemiology, 167, 280-286, doi: 10.1093/aje/kwm308, 2008.
980 Tan, H., Liu, L., Fan, S., Li, F., Yin, Y., Cai, M., and Chan, P. W.: Aerosol optical properties and
981 mixing state of black carbon in the Pearl River Delta, China, Atmos. Environ., 131, 196-208, doi:
982 10.1016/j.atmosenv.2016.02.003, 2016.
983 Tao, W. K., Chen, J. P., Li, Z. Q., Wang, C., and Zhang, C. D.: Impact of Aerosols on Convective
984 Clouds and Precipitation, Rev Geophys, 50, Rg2001, doi: 10.1029/2011rg000369, 2012.
985 Tasoglou, A., Saliba, G., Subramanian, R., and Pandis, S. N.: Absorption of chemically aged biomass
986 burning carbonaceous aerosol, J. Aerosol. Sci., 113, 141-152, doi: 10.1016/j.jaerosci.2017.07.011,
987 2017.
988 Tavakoli, F. and Olfert, J. S.: Determination of particle mass, effective density, mass–mobility
989 exponent, and dynamic shape factor using an aerodynamic aerosol classifier and a differential mobility
990 analyzer in tandem, J. Aerosol. Sci., 75, 35-42, doi: 10.1016/j.jaerosci.2014.04.010, 2014.

ten Brink, H., Otjes, R., Jongejan, P., and Slanina, S.: An instrument for semi-continuous monitoring of the size-distribution of nitrate, ammonium, sulphate and chloride in aerosol, Atmos. Environ., 41, 2768-2779, doi: 10.1016/j.atmosenv.2006.11.041, 2007.
Turpin, B. J. and Huntzicker, J. J.: Secondary Formation of Organic Aerosol in the Los-Angeles Basin - a Descriptive Analysis of Organic and Elemental Carbon Concentrations, Atmos. Environ., 25, 207-215, doi: 10.1016/0960-1686(91)90291-E, 1991.
Ueda, S., Nakayama, T., Taketani, F., Adachi, K., Matsuki, A., Iwamoto, Y., Sadanaga, Y., and Matsumi, Y.: Light absorption and morphological properties of soot-containing aerosols observed at an East Asian outflow site, Noto Peninsula, Japan, Atmos. Chem. Phys., 16, 2525-2541, doi: 10.5194/acp-16-2525-2016, 2016.
Virkkula, A., Makela, T., Hillamo, R., Yli-Tuomi, T., Hirsikko, A., Hameri, K., and Koponen, I. K.: A simple procedure for correcting loading effects of aethalometer data, J. Air Waste Manage. Assoc., 57, 1214-1222, doi: 10.3155/1047-3289.57.10.1214, 2007.
Wang, Q., Huang, R., Zhao, Z., Cao, J., Ni, H., Tie, X., Zhu, C., Shen, Z., Wang, M., and Dai, W.: Effects of photochemical oxidation on the mixing state and light absorption of black carbon in the urban atmosphere of China, Environmental Research Letters, 12, 044012, 2017.
Wang, Q. Y., Huang, R. J., Cao, J. J., Han, Y. M., Wang, G. H., Li, G. H., Wang, Y. C., Dai, W. T., Zhang, R. J., and Zhou, Y. Q.: Mixing State of Black Carbon Aerosol in a Heavily Polluted Urban Area of China: Implications for Light Absorption Enhancement, Aerosol. Sci. Technol., 48, 689-697, doi: 10.1080/02786826.2014.917758, 2014.
Wang, Y., Chung, A., and Paulson, S. E.: The effect of metal salts on quantification of elemental and organic carbon in diesel exhaust particles using thermal-optical evolved gas analysis, Atmos. Chem. Phys., 10, 11447-11457, doi: 10.5194/acp-10-11447-2010, 2010.
Wang, Y. Q.: MeteoInfo: GIS software for meteorological data visualization and analysis, Meteorological Applications, 21, 360-368, doi: 10.1002/met.1345, 2014.
Weingartner, E., Saathoff, H., Schnaiter, M., Streit, N., Bitnar, B., and Baltensperger, U.: Absorption of light by soot particles: determination of the absorption coefficient by means of aethalometers, J. Aerosol. Sci., 34, 1445-1463, doi: 10.1016/S0021-8502(03)00359-8, 2003.
Weyant, C. L., Shepson, P. B., Subramanian, R., Cambaliza, M. O. L., Heimburger, A., McCabe, D., Baum, E., Stirm, B. H., and Bond, T. C.: Black Carbon Emissions from Associated Natural Gas Flaring, Environ. Sci. Technol., 50, 2075-2081, doi: 10.1021/acs.est.5b04712, 2016.
Wild, M.: Enlightening Global Dimming and Brightening, B Am Meteorol Soc, 93, 27-37, doi: 10.1175/bams-d-11-00074.1, 2011.
Wu, C., Ng, W. M., Huang, J., Wu, D., and Yu, J. Z.: Determination of Elemental and Organic Carbon in PM2.5 in the Pearl River Delta Region: Inter-Instrument (Sunset vs. DRI Model 2001 Thermal/Optical Carbon Analyzer) and Inter-Protocol Comparisons (IMPROVE vs. ACE-Asia Protocol), Aerosol. Sci. Technol., 46, 610-621, doi: 10.1080/02786826.2011.649313, 2012.
Wu, C., Huang, X. H. H., Ng, W. M., Griffith, S. M., and Yu, J. Z.: Inter-comparison of NIOSH and IMPROVE protocols for OC and EC determination: implications for inter-protocol data conversion, Atmos. Meas. Tech., 9, 4547-4560, doi: 10.5194/amt-9-4547-2016, 2016a.

Wu, C. and Yu, J. Z.: Determination of primary combustion source organic carbon-to-elemental carbon (OC/EC) ratio using ambient OC and EC measurements: secondary OC-EC correlation minimization method, Atmos. Chem. Phys., 16, 5453-5465, doi: 10.5194/acp-16-5453-2016, 2016.
Wu, D., Mao, J. T., Deng, X. J., Tie, X. X., Zhang, Y. H., Zeng, L. M., Li, F., Tan, H. B., Bi, X. Y., Huang, X. Y., Chen, J., and Deng, T.: Black carbon aerosols and their radiative properties in the Pearl River Delta region, Sci China Ser D, 52, 1152-1163, doi: 10.1007/s11430-009-0115-y, 2009.
Wu, D., Wu, C., Liao, B., Chen, H., Wu, M., Li, F., Tan, H., Deng, T., Li, H., Jiang, D., and Yu, J. Z.: Black carbon over the South China Sea and in various continental locations in South China, Atmos. Chem. Phys., 13, 12257-12270, doi: 10.5194/acp-13-12257-2013, 2013.
Wu, Y., Zhang, R., Tian, P., Tao, J., Hsu, S. C., Yan, P., Wang, Q., Cao, J., Zhang, X., and Xia, X.: Effect of ambient humidity on the light absorption amplification of black carbon in Beijing during January 2013, Atmos. Environ., 124, Part B, 217-223, doi: 10.1016/j.atmosenv.2015.04.041, 2016b.
Yang, M., Howell, S. G., Zhuang, J., and Huebert, B. J.: Attribution of aerosol light absorption to black carbon, brown carbon, and dust in China - interpretations of atmospheric measurements during EAST-AIRE, Atmos. Chem. Phys., 9, 2035-2050, doi: 10.5194/acp-9-2035-2009, 2009.
Yu, H., Wu, C., Wu, D., and Yu, J. Z.: Size distributions of elemental carbon and its contribution to light extinction in urban and rural locations in the pearl river delta region, China, Atmos. Chem. Phys., 10, 5107-5119, doi: 10.5194/acp-10-5107-2010, 2010.
Yuan, J. F., Huang, X. F., Cao, L. M., Cui, J., Zhu, Q., Huang, C. N., Lan, Z. J., and He, L. Y.: Light absorption of brown carbon aerosol in the PRD region of China, Atmos. Chem. Phys., 16, 1433-1443, doi: 10.5194/acp-16-1433-2016, 2016.
Zhang, G., Bi, X., Qiu, N., Han, B., Lin, Q., Peng, L., Chen, D., Wang, X., Peng, P., Sheng, G., and Zhou, Z.: The real part of the refractive indices and effective densities for chemically segregated ambient aerosols in Guangzhou measured by a single-particle aerosol mass spectrometer, Atmos. Chem. Phys., 16, 2631-2640, doi: 10.5194/acp-16-2631-2016, 2016a.
Zhang, R. Y., Khalizov, A. F., Pagels, J., Zhang, D., Xue, H. X., and McMurry, P. H.: Variability in morphology, hygroscopicity, and optical properties of soot aerosols during atmospheric processing, P Natl Acad Sci USA, 105, 10291-10296, doi: 10.1073/pnas.0804860105, 2008.
Zhang, Y., Zhang, Q., Cheng, Y., Su, H., Kecorius, S., Wang, Z., Wu, Z., Hu, M., Zhu, T., Wiedensohler, A., and He, K.: Measuring the morphology and density of internally mixed black carbon with SP2 and VTDMA: new insight into the absorption enhancement of black carbon in the atmosphere, Atmos. Meas. Tech., 9, 1833-1843, doi: 10.5194/amt-9-1833-2016, 2016b.

1065 Table 1. Abbreviations.

1066

Abbreviation	Definition
$AAE_{470\text{-}660}$	Absorption Angstrom Exponent between 470 and 660 nm
BB	Biomass burning
BrC	Brown Carbon
D_{core}, D_{shell}	Particle diameter of core/shell
E_{abs550}	Light absorption enhancement factor at 550 nm
σ_{abs550}	Light absorption coefficient at 550 nm
$\sigma_{abs,t}$	Total light absorption coefficient of a coated particle
$\sigma_{abs,p}$	Primary light absorption coefficient attributed to the soot core alone of a coated particle
$\sigma_{abs,c}$	Extra light absorption coefficient due to the lensing effect of coating on the soot core
LII	Laser induced incandescence technique for soot measurement
LWC	Liquid water content
MAE_{550}	Mass absorption efficiency at 550 nm, also known as mass absorption cross-section (MAC)
$MAE_{p,550}$	Primary MAE of freshly emitted soot particles at 550 nm
MAAP	Multi Angle Absorption Photometer
MOUDI	Micro Orifice Uniform Deposit Impactor
MRS	Minimum R squared method
PAS	Photo acoustic spectrometer
PRD	Pearl River Delta region, China
SP2	Single particle soot photometer
SSA	Single scattering albedo
TD	Thermal denuder
TOA	Thermal optical analysis
TSV	Total spatial variance in backward trajectories cluster analysis

1067

1068 Table 2. Comparison of MRS application on $(OC/EC)_p$ (for SOC estimation) and MAE_p (for E_{abs} estimation).

1069

	MRS in EC tracer method for SOC estimation (Wu and Yu, 2016)	**MRS in EC tracer method for E_{abs} estimation (this study)**
Key parameter of fresh EC particles to be determined	$(\frac{OC}{EC})_p = \frac{POC}{EC}$	$MAE_p = \frac{\sigma_{abs,p}}{EC}$
Input quantities for MRS from measurements	OC, EC (tracer)	$\sigma_{abs,t}$, EC (tracer)
Variable to be decoupled by the tracer	$OC = POC + SOC$ $= (\frac{OC}{EC})_p \times EC + SOC$	$\sigma_{abs,t} = \sigma_{abs,p} + \sigma_{abs,c}$ $= \frac{\sigma_{abs,p}}{EC} \times EC + \sigma_{abs,c}$
Ambient measurement at its closest to fresh emissions	Minimum R^2 (SOC, EC) $SOC = OC - (\frac{OC}{EC})_p \times EC$	Minimum R^2 ($\sigma_{abs,c}$, EC) $\sigma_{abs,c} = \sigma_{abs,t} - MAE_p \times EC$
Graph	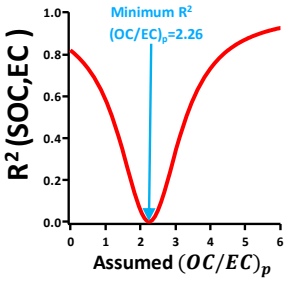	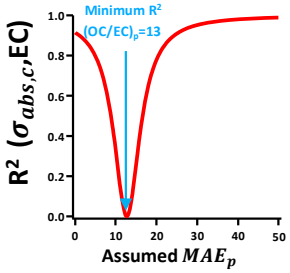

1070

1071 Table 3. Comparison of E_{abs} between various studies.

1072

Location	Type	Sampling Duration	λ (nm)	Instrument	E_{abs}	Method	Reference
Guangzhou, China	Suburban	2012.2-2013.1	550	AE+OCEC	1.50±0.48	MAE	This study
Xi'an, China	Urban	2012.12-2013.1	870	PAS	1.8	MAE	(Wang et al., 2014)
Shenzhen, China	Urban	2011.8-9	532	PAS	1.3	MAE	(Lan et al., 2013)
Jinan, China	Urban	2014.2	678	OCEC	2.07 ± 0.72	AFD	(Chen et al., 2017)
Nanjing, China	Suburban	2012.11	532	PAS	1.6	MAE	(Cui et al., 2016a)
Boulder, USA	Forest fire	2010.9	532	PAS	1.38	TD 200°C	(Lack et al., 2012a)
London, UK	Rural	2012.2	781	PAS	1.4	TD 250°C	(Liu et al., 2015)
California, USA	Rural	2010.6	532	PAS	1.06	TD 250°C	(Cappa et al., 2012)
Noto Peninsula, Japan	Rural	2013.4-5	781	PAS	1.22	TD 300°C	(Ueda et al., 2016)
Yuncheng, China	Rural	2014.6-7	678	OCEC	2.25 ± 0.55	AFD	(Cui et al., 2016b)
San Jose, Costa Rica	Rural	2006 winter	1064	SP2	1.3	Mie+SP2	(Schwarz et al., 2008)

1073 AE: Aethalometer ; OCEC: OCEC analyzer; PAS: photo acoustic spectrometer; SP2: Single particle soot photometer; TD: Thermal
1074 denuder AFD: filter filtration-dissolution

1075

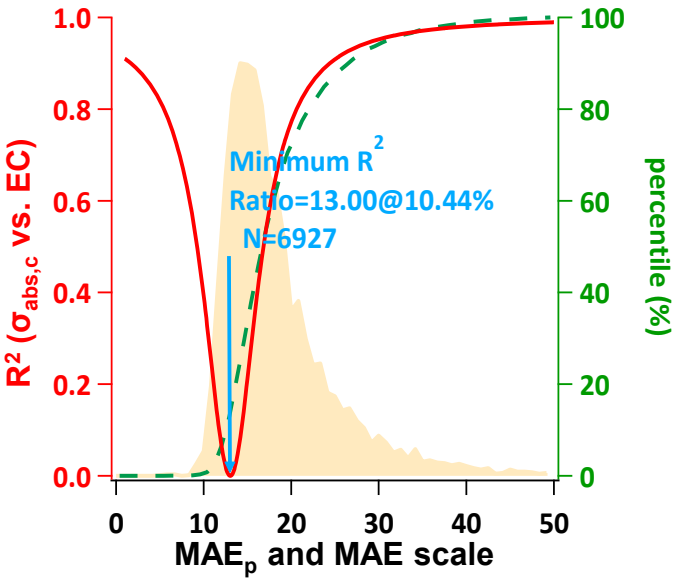

Figure 1. Minimum R squared (MRS) plot for calculating MAE_p at 550 nm. The red curve is the correlation result between $\sigma_{abs,c}$ ($\sigma_{abs,t}$ – EC * MAE_p) and EC mass. The shaded area in light tan represents the frequency distribution of observed MAE. The dashed green line is the cumulative distribution of observed MAE.

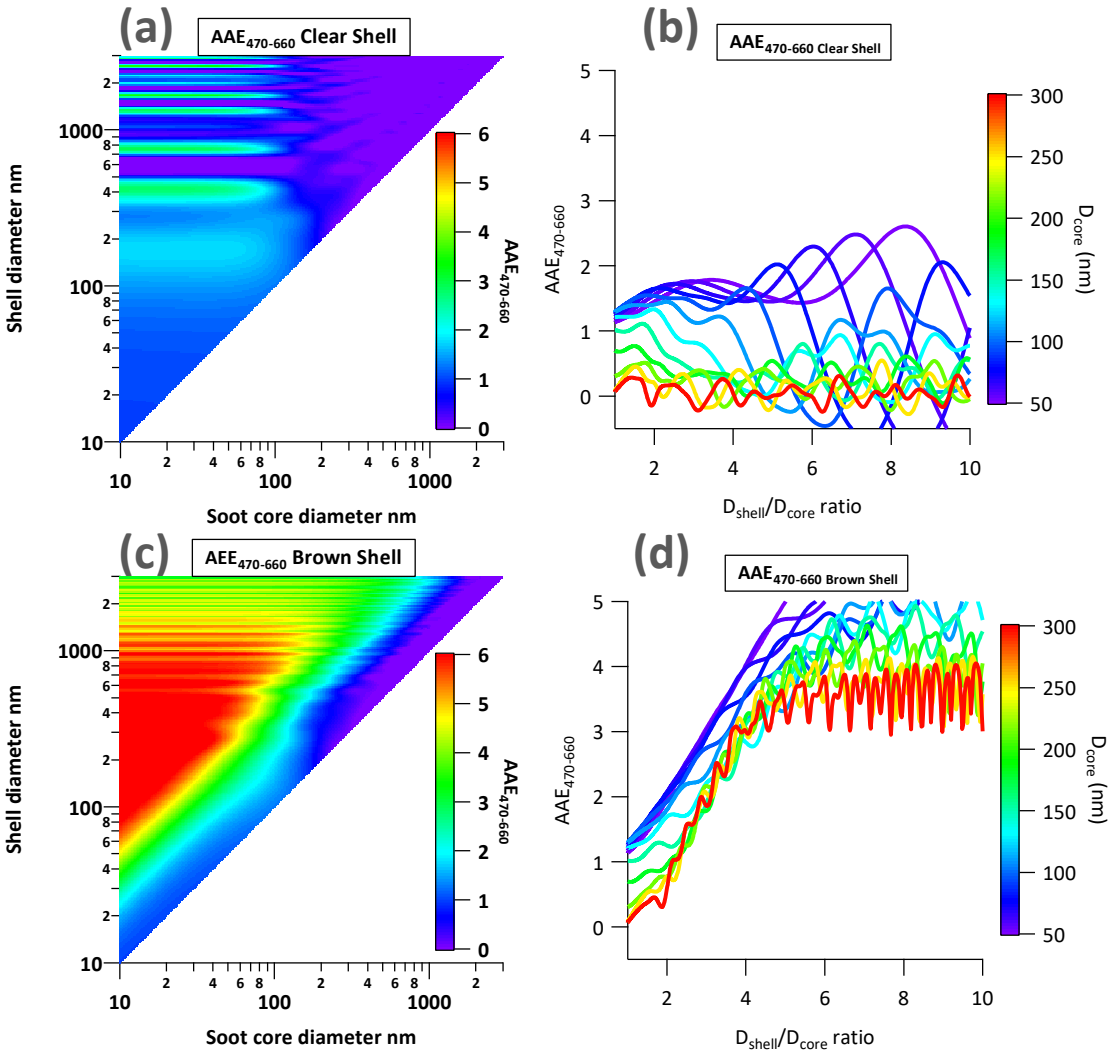

Figure 2. Mie simulated size dependency of soot particles $AAE_{470\text{-}660}$. (a) Combination of different clear shell (y axis) and core diameters (x axis). The color coding represents the $AAE_{470\text{-}660}$ of a particle with specific core and clear shell size; (b) Cross-sections views of (a). The color coding represents different D_{core} in the range of 50 ~ 300 nm. (c)&(d) Similar to (a)&(b) but from the brown shell scenario.

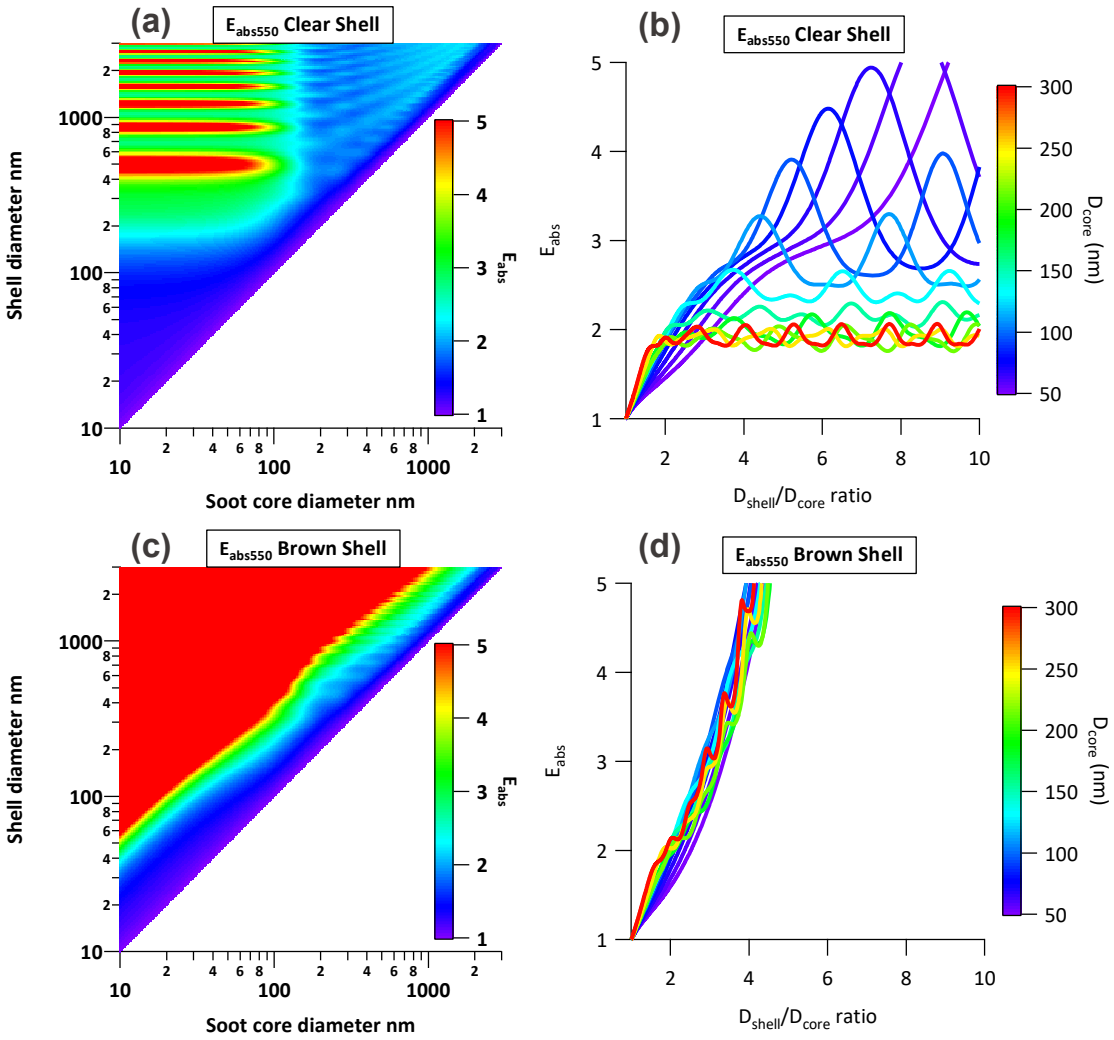

Figure 3. Mie simulated size dependency of soot particles E_{abs} at wavelength 550 nm. (a) Combination of different clear shell (y axis) and core diameters (x axis). The color coding represents the E_{abs} of a particle with specific core and clear shell size; (b) Cross-sections views of (a). The color coding represents different D_{core} in the range of 50 – 300 nm. (c)&(d) Similar to (a)&(b) but from the brown shell scenario.

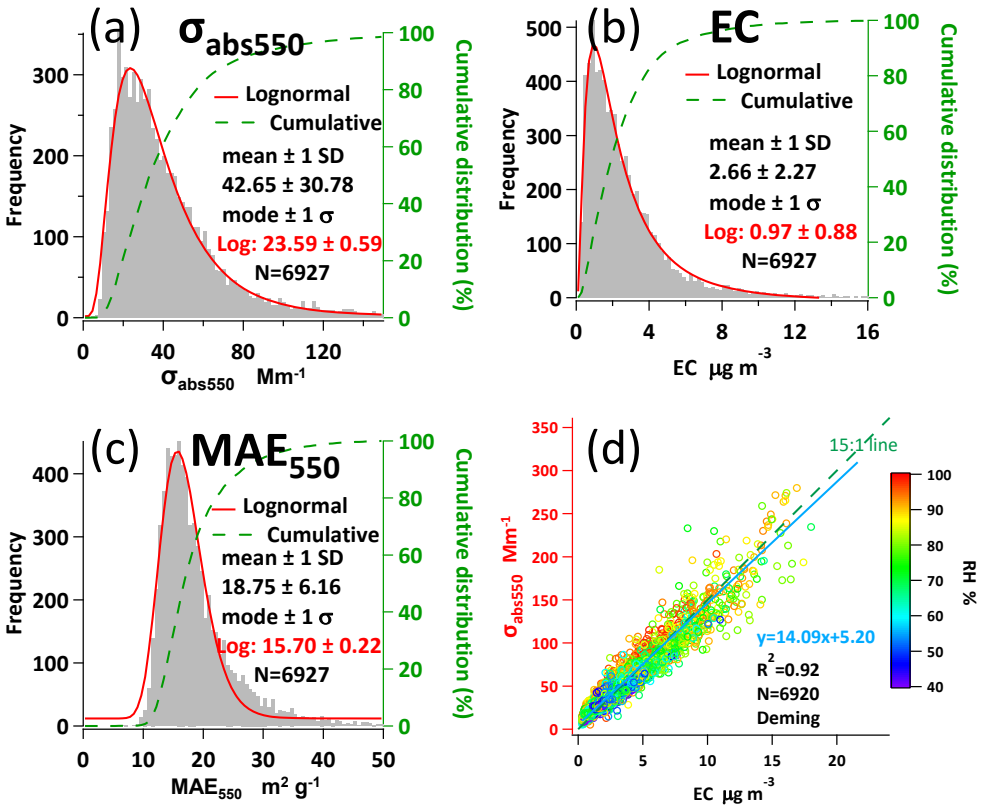

Figure 4. Measured annual statistics of σ_{abs550} , EC and MAE_{550}. (a) Annual frequency distribution of light absorption at 550 nm. The red curve represents the fitting line for a log-normal distribution. (b) Annual frequency distribution of EC mass concentration (c) Frequency distribution of Mass absorption efficiency (MAE) at 550 nm. (d) Scatter plot of light absorption (550 nm) and EC mass. The slope represents MAE_{550}. The blue regression line is by Deming regression. The color coding represents RH.

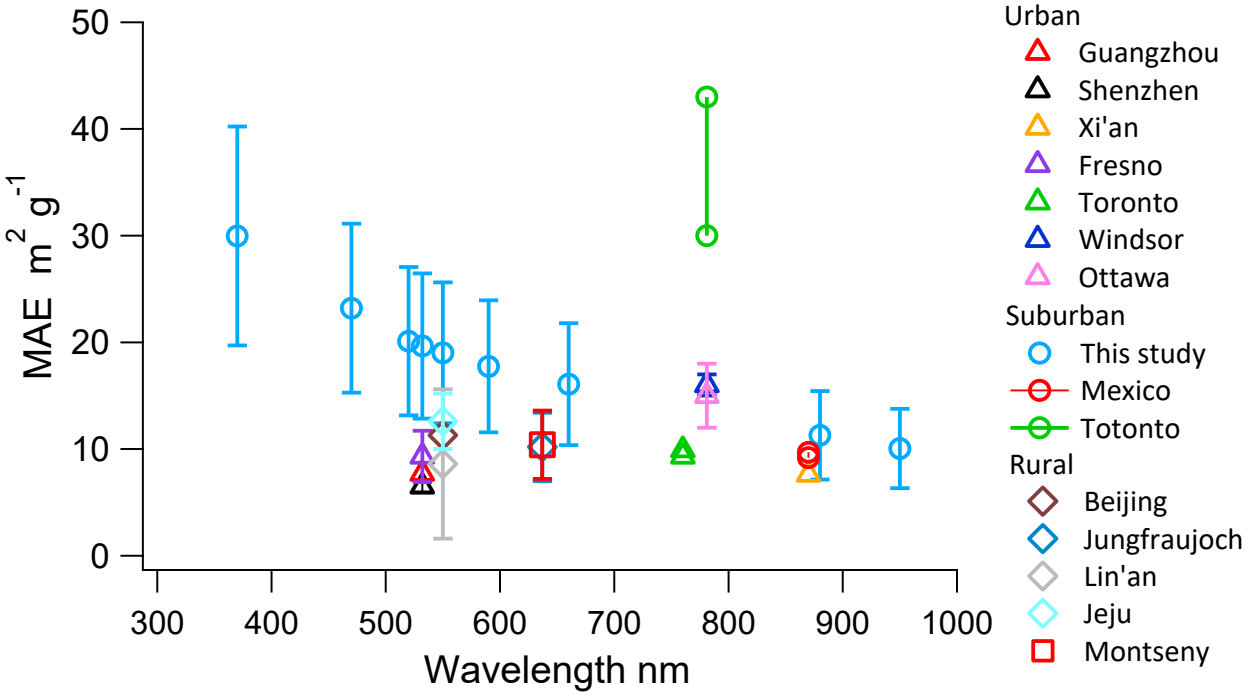

1103

1104 Figure 5. Comparison of spectral MAE measurements from this study with previous studies. Triangle, circle and rhombus
1105 represent urban, suburban and rural respectively. Details and reference can be found in Table S1. The whiskers represent
1106 one standard deviation.

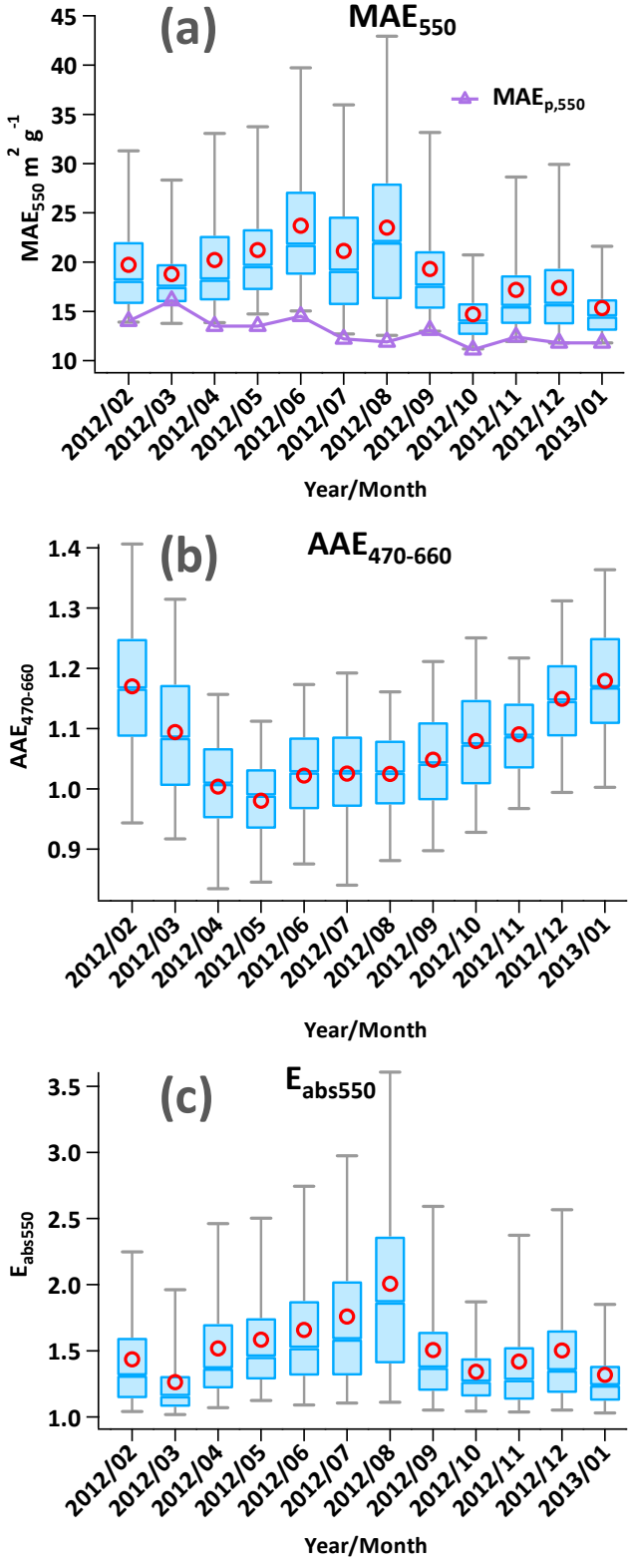

Figure 6. Measured monthly variations of (a) MAE_{550}, the purple line represents $MAE_{p,550}$ estimated by MRS (b) $AAE_{470-660}$ and (c) E_{abs550}. Red circles represent the monthly average. The line inside the box indicates the monthly median. Upper and lower boundaries of the box represent the 75th and the 25th percentiles; the whiskers above and below each box represent the 95th and 5th percentiles.

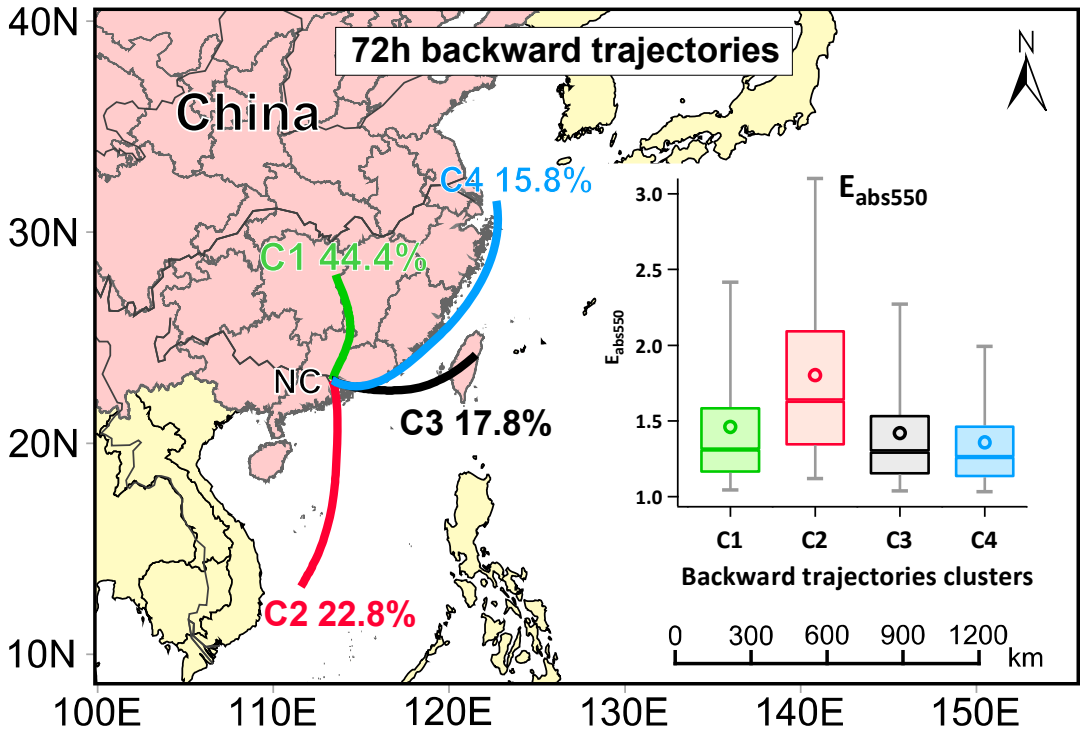

Figure 7. Average backward trajectories arriving at 100 m at NC site for four clusters (2012 Feb - 2013 Jan). E_{abs550} by different clusters are shown in the box plot.

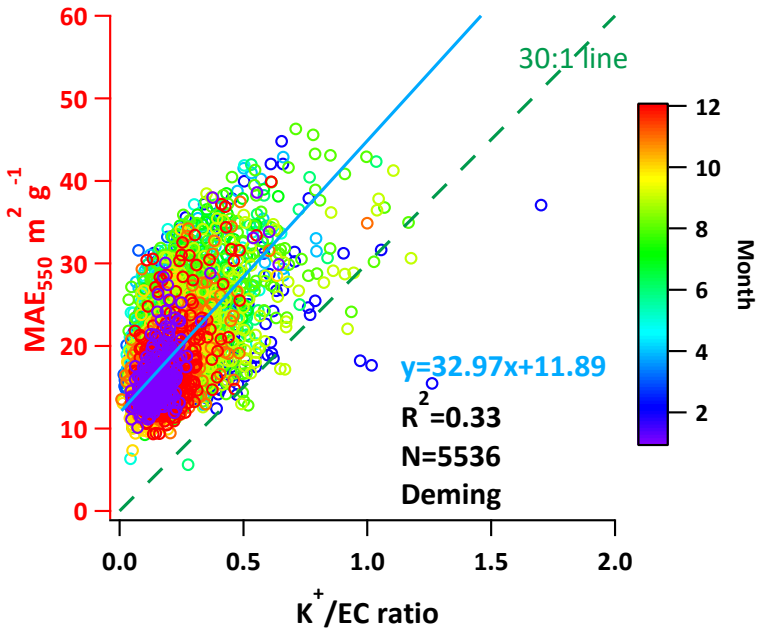

Figure 8. MAE_{550} dependency on biomass burning indicator K^+/EC ratio. The color coding represents months. The intercept represents MAE without biomass burning effect. The 30:1 line serves as a reference line with an integer slope that is close to the regressed slope through the origin.